Rocco Sorace

Development and Analysis of Proton Exchange Membrane Water Electrolyzer (PEMWE) Model with Chemical Degradation Phenomenon

Master's thesis

◻ NTNU
Norwegian University of
Science and Technology

Rocco Sorace

Development and Analysis of Proton Exchange Membrane Water Electrolyzer (PEMWE) Model with Chemical Degradation Phenomenon

NTNU

Norwegian University of
Science and Technology

Abstract

The Green House Gas emissions represent an ongoing global issue, pushing countries all over the world towards an increased interest in the renewable energy sources. In this direction, an efficient energy storage system is required to deal with their intermittent operations. To address such challenge, Hydrogen can be considered as a good candidate for renewable energy storage. In this thesis, a detailed literature review is conducted to study different hydrogen production technologies. As a result, an important component for the connection between Hydrogen and the renewable resources is found out to be the water electrolyzer. Therefore, in the proposed work, a detailed model of a Proton Exchange Membrane Water Electrolyzer (PEMWE) and the chemical degradation phenomenon of PEMWE is analyzed.

In particular, a mathematical model of PEMWE operation at steady state is developed. Simulations are performed by varying the operating conditions (temperature, current density and pressure) and the effect on the cell voltage is examined in MATLAB® environment. In addition, a chemical degradation model is analyzed to study the membrane dissolution in absence of metal-ions impurities source, showing the influence of the operating parameters on the degradation phenomena.

Moreover, contribution to research activities and foundation for further optimizations of PEM water electolyzers are the major outcomes of this work. These activities are performed as a part of Clean Energy Export research project that exploits Norway's potential for future energy export to Europe.

Sammendrag

Klimagassutslipp representerer en pågående global problemstilling som presser land over hele verden mot en økning av mengden energi produsert av fornybare energikilder. For å håndtere at fornybare energikilder generelt ikke opererer hele tiden kreves et effektivt energilagringssystem. Hydrogen betraktes som en god kandidat for lagring av fornybar energi. I denne avhandlingen gjennomføres en detaljert litteraturgjennomgang for å studere forskjellige hydrogenproduksjonsteknologier. Det har vist seg at vannelektrolysatoren spiller en viktig rolle for fornybare ressurser basert på hydrogen. Derfor blir det i dette arbeidet analysert en detaljert modell av en Proton Exchange Membrane Water Electrolyzer (PEMWE) og det kjemiske nedbrytningsfenomenet PEMWE.

Spesielt utvikles en matematisk modell for PEMWE-drift i steady state. Simuleringer utføres ved å variere driftsforholdene (temperatur, strømtetthet og trykk) og effekten på cellespenningen undersøkes ved bruk av MATLAB®. I tillegg analyseres en kjemisk nedbrytingsmodell for å studere membranoppløsningen i fravær av kilder til metallioniske urenheter. Dette viste innflytelsen fra driftsparametrene på nedbrytningsfenomenet.

De viktigste resultatene av dette arbeidet er bidragene til forskningsaktiviteter og grunnlag for ytterligere optimalisering av PEM vannelektolysatorer. Disse aktivitetene utføres som en del av forskningsprosjektet Clean Energy Export som utnytter Norges potensiale for fremtidig energieksport til Europa.

Acknowledgments

This Master's thesis allowed me to increase my knowledges and expertise in one of my field of interest and it has been possible thanks for the constant guidance and support of several people to whom I want to express my sincere gratitude.

I would like to begin by saying thank to my main supervisor, Associate Professor Lars Olof Nord, without whom my whole Erasmus experience wouldn't be feasible. I'm grateful for the patience, for the openness and for the always useful and wise advice in the work and for my future carrier.

Secondly, I will be forever thankful to my co-supervisor, Postdoctoral Fellow Gaurav Mirlekar, for the continuous collaborations, help and exchange of opinions, thanks to which I could professionally and culturally grow.

Finally, a special appreciation must be addressed to my family for encouragement and significant financial support, as well as to my friends for the fundamental moral backing.

x

Table of Contents

List of Figures

List of Tables

List of Abbreviations

AEC	Alkaline Electrolyzer Cell
CAPEX	Capital Expenditure
CCUS	Carbon Capture Utilization and Storage
CEE	Clean Energy Export
EPT	Department of Energy and Process Engineering
FRR	Fluoride Release Rate
GDL	Gas Diffusion Layer
HOR	Hydrogen Oxidation Reaction
HT	High Temperature
IEA	International Energy Agency
IEAGHG	International Energy Agency Green House Gas
LT	Low Temperature
MEA	Membrane Electrode Assembly
NTNU	The Norwegian University of Science and Technology
OCV	Open Circuit Voltage
OPEX	Operating Expense
ORR	Oxygen Reduction Reaction
PEMEC	Proton Exchange Membrane Electrolyzer Cell
PEMFC	Proton Exchange Membrane Fuel Cell
PEMWE	Proton Exchange Membrane Water Electrolyzer
POX	Partial Oxidation
PV	Photovoltaic
RES	Renewable Energy Sources
SINTEF	Foundation for Scientific and Industrial Research Selskapet for Industrial og Teknisk Forskning
SMR	Steam Methane Reforming
SOEC	Solid Oxide Electrolyzer Cell
TR	Thinning Rate
WGS	Water Gas Shift

1 Introduction

With a growing awareness and interest in sustainable energy system an increasing number of countries are setting ambitious goals with the aim of reducing greenhouse gases emissions and the related increase of global temperature. This is the case of the European Union that, as stated in the European Green Deal (European Commission, 2019), aspire to the climate neutrality by 2050 compared with 1990 levels. In order to reach this objective an important intervention on the energy system is needed and in this transition Hydrogen will have a key role.

The International Energy Agency (IEA) in its report for the G20 in Japan, *The Future of Hydrogen* (IEA, 2019), highlights the relevance and the opportunities of this low-carbon chemical energy carrier as a leading option to decrease the emissions. Its properties of being stored, involved in combustion and in chemical reactions are similar to the common fossil fuel (natural gas, oil and coal).

The opportunities of H_2 range from road transport to steel production to energy application (industry, transport, heating, cooling, power generation, etc.). Its variability (SBC Energy Institute, 2014) can help energy balancing on a system level providing with both temporal and geographic flexibility in a pathway consistent with rising shares of renewables, as well as it can assure energy security.

As pointed out in the special report above mentioned, it has been already displayed the feasibility of the conversion of electricity into Hydrogen and back or further converted to other fuels. As a consequence, end users will be less dependent on specific energy resources and the energy supplies resilience will grow (IEA, 2019).

Moreover, high energy density of Hydrogen makes this element suitable for MWh to TWh storages, such as pressurized cylinders or underground in salt caverns, depleted oil and gas reservoirs and saline aquifers (F. Zhang et al., 2016). By means of a conversion of electricity into hydrogen, this chemical energy carrier can match the variable energy supply and demand, smoothing peaks and valley. Eventually, facing the main issue of variable renewable energy sources, it can boost their diffusion.

Concerning transport sector, Hydrogen is gaining success as a low-carbon fuel for long ranges, such as road freight, rail and shipping (Brandon & Kurban, 2017).Indeed, it can be used in combustion engine or providing electricity to electrical vehicles using fuel cell technologies.

In the near-term scenario, blending Hydrogen in the existing natural gas network is a real opportunity. (IEA, 2019) reports that the low-concentration, low-carbon, blending path could help reducing emissions, estimating, for the 2030, a use of Hydrogen potentially up to 4 Mt just for heating buildings. Its potential is seen considering the dense cities, as well as multifamily and commercial buildings. Here, the transition to the use of heat pump is more challenging. In addition, the same report of the International Agency proposes, for longer-term prospect, Hydrogen directly used in boilers or fuel cells in the heating network. In any case, it is also highlighted the need of infrastructure upgrades and of safety studies to provide public reassurance.

Even though nowadays it has a marginal role in power generation, Hydrogen use could be interesting, also, in combination with ammonia, to reduce carbon emissions in the existing coal power plants or for hydrogen-fired gas turbines and combined-cycle gas turbines.

Therefore, Hydrogen can be considered a great opportunity for simultaneous and multi-sectoral decarbonization, leading to a more flexible electric system. An increase of the efficiency of decarbonization indeed results from the encouraged spread of variable renewable energy sources as well as of the creation of new paths connecting different energy carriers (i.e. electricity, gas and heating) with different final uses (IEA, 2020a).

1.1 Background

The proposed work is part of the Clean Energy Export (CEE) research project, developed by SINTEF Energy with support from the Department of Energy and Process Engineering (EPT) at the Norwegian University of Science and Technologies (NTNU). The aim of the CEE is to provide strategic guidance and investment support for exploiting Norway's potential for future clean energy export to Europe.

The Norwegian energy system could rely on two flexible energy sources: hydropower and natural gas. This flexibility will place the country "in a unique position in the long-term perspective, when renewable intermittent power production will become a larger part of the European energy supply"(Skar et al., 2018).

The production in Norway is in considerable surplus with respect to the total energy consumption (almost ten times in the 2018,(IEA, 2020b)), but new wind farm and small-scale solar power are plan to be built as stated by Caroline Østlie. The head of the Strategic Market Analysis unit in Statkraft, leading company in hydropower and Europe's largest generator of renewable energy, affirmed that around 20 TWh to 30 TWh of wind power is under construction or licensed in the Norwegian and Swedish regions. Moreover, an upgrading of the existing generation facilities is expected concurrently to the construction of small-scale power plants (*Energy: Do We Have Enough Power to Face the Future?*, 2019).

As a result, this new production is intended to be exported to the neighboring countries, directly on the electricity network or following other energy carrier, such as Hydrogen.

The main opportunities and challenges of CEE concerns cost-effective investment in new infrastructure, energy systems with intermittent energy production (e.g. renewable energy sources) as well as increasing data requirements and improvement of data quality.

Under this research path, the following work is analyzed for Hydrogen production technologies.

1.2 Proposed Work

1.2.1   Purpose

The following work aims to set the basis for an optimization of the Proton Exchange Membrane (PEM) Water Electrolyzer (PEMWE) technologies in term of variation of the operative conditions of temperature, current density and pressure considering the degradation phenomena. In order to accomplish this target, after a detailed literature review of the equations linked to this device, a mathematical model is developed in the MATLAB® environment. Thus, as main purpose of the thesis, a sensitivity analysis is presented varying the above-mentioned parameters.

1.2.2   Limitation of the scope

The thesis presents several limitations in terms of analysis and approach to the modelling. Using the sub-categorization of the different modelling approaches suggested by (Gao et al., 2012), the work is focusing only on zero-dimensional, steady state models, where analytical and semi-empirical equations are combined on single cell and stack model area to describe

electrochemical and chemical phenomena. The scheme of the mentioned limitations is described in the figure 1-1.
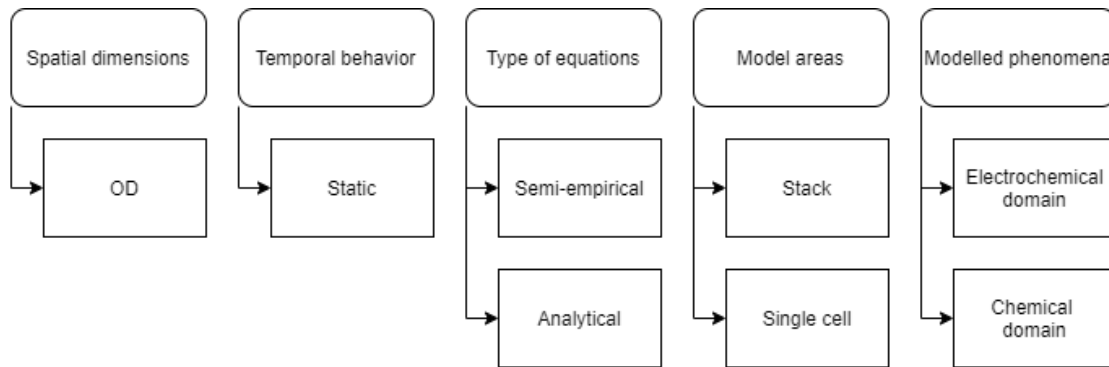
Figure 1-1 Model classification chart   redrawn in the paper according to the sub-categorization of (Gao et al., 2012)

1.2.3   Objectives

The purpose described before is further subdivided and pursued by means of the following work objectives:

- Conduct thorough literature review of the state-of-art Hydrogen production technologies and select the optimal method.
- Study the phenomena and models proposed in the open literature of the PEM Electrolyzers and its degradation.
- Develop a simplified model to be implemented in the MATLAB® environment.
- Perform a sensitivity analysis of the performance of the PEMWE.

1.2.4   Research Approach

The thesis results from the following research path:

- Collaboration with the co-supervisor Postdoctoral Fellow Gaurav Mirlekar from the beginning to the deadline of the master's thesis, as well as with the supervisor Associate Professor Lars O. Nord.
- Additional meetings with the research group of supervisor Associate Professor Lars O. Nord.
- Thorough literature review of the technologies and models.
- Screening of the technologies.
- Process modeling and simulation.

1.2.5   Contribution

The contribution given by this work consists in providing a description of the current results in modelling and understanding the phenomena of the PEM electrolyzer, in suggesting a possible simulation and analysis as a

starting point for a successive optimization, missing in the literature for this device.

1.3 Organization of the Thesis

The structure of the thesis consists of five chapters. In the first chapter, to which this section belongs, the topic of Hydrogen production and current status is introduced as well as the motivation and the origin of the thesis is explained. The second chapter aims to show the state-of-art of the Hydrogen technologies for different sources and processes, concluding with a confrontation of such method. Selected the optimal technology, its mathematical modelling and electrochemical phenomena and chemical degradation issue are explained in the third chapter. The fourth chapter is, thus, dedicated to the discussion of the results and to the sensitivity analysis. Finally, the conclusions and possible further works are presented in the fifth chapter.

2 Technologies for Hydrogen production

Hydrogen production can follow several paths, employing different energy sources and technologies, from fossil fuels, to biomass or water.
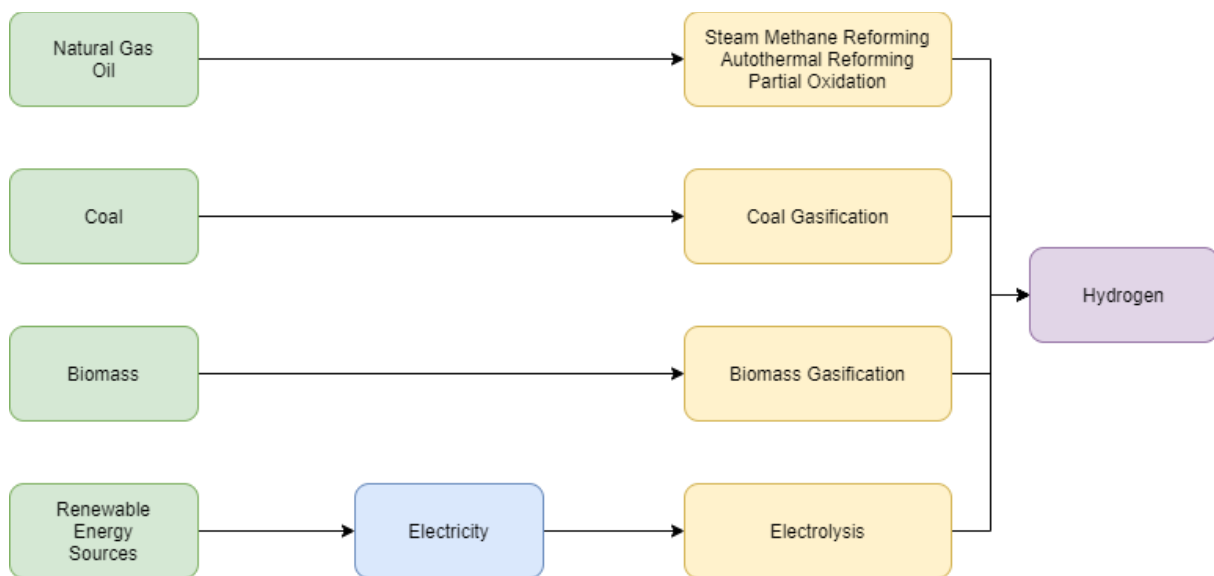
Figure 2-1 Prevalent pathways for producing Hydrogen

Nowadays, the required Hydrogen in its pure form, 70 MtH_2/year (IEA, 2019), is supplied mainly by fossil fuels (in Europe 90,6% of Hydrogen according to the Clean Hydrogen Monitor produced by EU in 2020 (Hydrogen Europe, 2020)). Around the world, Natural gas, by means of reforming processes, counts for the 76% whereas coal covers the 23% through coal gasification. However, green hydrogen, produced by renewable energy sources by means of water electrolytic processes, is gaining attention due to the decrease of renewable power cost, in particular solar photovoltaic (PV) and wind power.

Considering the high dependence on fossil fuels, it is clear how the H_2 production is connected to a high level of CO_2 emissions: 830 $MtCO_2$/year, as reported by the International Energy Agency (IEA, 2019),

considering the cumulative emissions of natural gas (10 tCO₂/tH₂), oil products (12 tCO₂/tH₂) and coal (19 tCO₂/tH₂).

2.1 Hydrogen from natural gas

The compound behind the utilization of natural gas as a source for the production of Hydrogen is the methane (CH_4) which can be treated with thermal processes such as Steam Methane Reforming (SMR), Partial Oxidation and a combination of them: Autothermal Reforming (ATR).

2.1.1   Steam Methane Reforming (SMR)

SMR represents the main method for Hydrogen production. As shown in the equation (2.1), this process, already mature, consists in a reaction of a high-temperature steam (500°C-900°C) under 3-25 bar of pressure, reacting with the methane, present in the natural gas. The products obtained are hydrogen, carbon monoxide and carbon dioxide in small quantity. The reaction occurs with a steam-to-carbon (S/C) ratios of 2.5-3.0 (Voldsund et al., 2016) and in presence of a catalyst, often with a Ni-based (having low cost and sufficient activity). The reaction is highly endothermic: it required heat for proceeding.

$$CH_4 + H_2O \rightleftharpoons CO + 3H_2 \quad \Delta H_{rx} = 206\frac{kJ}{mol} \qquad (2.1)$$
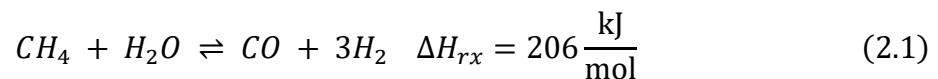
As a consequence, as highlighted by (Subramani et al., 2010), high temperatures, as well as low pressure and high S/C ratio, (positive for low carbon deposition, although negative for an energetic and economic side), facilitate the reaction.

After the reforming reaction, the carbon monoxide and the water, in steam phase, are involved in the "water-gas shift" reaction (WGS), reaction (2.2), producing carbon dioxide and additional hydrogen, through the use of a catalyst.

$$CO + H_2O \rightleftharpoons CO_2 + H_2 \quad \Delta H_{rx} = -41\frac{kJ}{mol} \qquad (2.2)$$
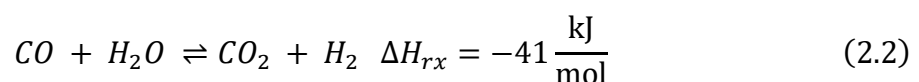
This reaction, slightly exothermic, is usually performed in two stages at different temperatures: High Temperature (HT) WGS at 320-360°C to boost the kinetics of the reaction and to reduce the catalyst bed volume, followed by the Low Temperature (LT) WGS at 190-250 °C favorizing high

conversion. The pressure in the two stages is respectively 10-60 bar and 10-40 bar: even if the total pressure does not influence the CO conversion, an higher pressure helps to increase the reaction rate (Mendes et al., 2010).

Pressure swing absorption is, then, the final process for the purification of Hydrogen from impurities.

SMR usually extracted hydrogen from natural gas, but it can be applied to liquefied petroleum gas (LPG), ethanol, propane, gasoline and naphtha. In these cases, a pre-reformer is required for converting the heavier hydrocarbon into methane and for its initial reforming into CO and H_2, at an operating temperature around 400-500°C (Ritter & Ebner, 2007).

2.1.2 Partial Oxidation (POX)

Partial Oxidation is defined as the reaction between the hydrocarbons in natural gas, in large part methane or heavy hydrocarbons (diesel fuel and residual oil), and a limited, sub-stoichiometric amount of oxygen (usually from air). The term *partial* refers to the insufficiency of the oxygen to obtain a complete oxidation of the hydrocarbons into carbon dioxide and water.

The products, on view in the equation (2.3), are mainly carbon monoxide and hydrogen. In case the oxygen used comes from air, also Nitrogen is present in the products and it must be processed downstream or used for ammonia production. The reaction can occur with or without the present of a catalyst.

In addition, relatively lower quantities of CO_2, other compounds and a small amount of heat is produced, (it is an exothermic reaction).

$$C_mH_n + \frac{m}{2}O_2 \rightleftharpoons mCO + \frac{n}{2}H_2 \qquad (2.3)$$
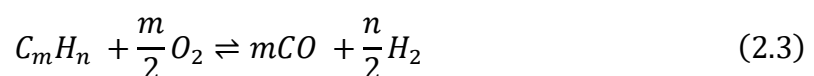
Next, following the same path for the steam methane reforming, the products of the previous reaction are involved in a water-gas shift reaction, displayed above in the equation (2.2), obtaining more H_2 and CO_2.

In general, the process of POX is much faster than SMR process, with shorter response times and smaller required size of the reactor vessel, more compact, with contact times of typically milliseconds (Wang & Rohr, 2002).

Moreover, partial oxidation process is more tolerant of high levels of sulfur contaminants in the HC fuels. However, the Hydrogen content of the reaction is low, and the operating temperature required by this technology

is high. These operating conditions can cause the degradation of the catalyst.

2.1.3   Autothermal Reforming (ATR)

Combining the endothermic nature of the Steam Methane Reforming and the exothermicity of the Partial Oxidation, Autothermal Reforming represents a more flexible process. It consists in the reaction between methane, oxygen and steam in a single chamber as follows:

$$CH_4 + \frac{1}{2} H_2O + \frac{1}{4} O_2 \rightleftharpoons CO + \frac{5}{2} H_2 \qquad \Delta H_{rx} = 84 \frac{kJ}{mol} \qquad (2.4)$$
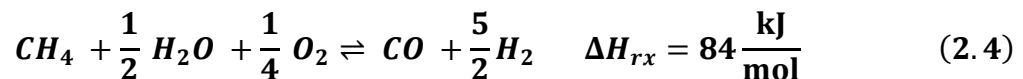
As a general concept, the heat produced by the POX reaction is used in the endothermic SMR reaction. The amount of steam and oxygen can be varied to control the operating temperature and the ratio between Hydrogen and carbon monoxide in the products. Usually, the process operate at 900-1500°C and 1-80 bar (Ke Liu, Deluga, et al., 2009).

Using the heat produced by the reformer itself implies that the CO_2 is obtained inside the reactor. Consequently, a higher CO_2 recovery rates can be achieved with respect to SMR, which is, then, less responsive. Moreover, considering that the emissions of ATR are more concentrated than SMR, the cost for capturing the emissions is lower, as well as the vessel size and weight requirements.

It is understandable that with a higher level of complexity, as a downside, it requires an extensive control system for the Autothermal Reforming, to guarantee the stability and the robustness in the operation of the fuel processing system.

However, it is interesting highlighting that the most mature technology, SMR, still appears to be a solution also for the next future. According to IEA special report, indeed, Steam Methane Reforming in the near term will remain the dominant technology for large-scale hydrogen production due to its advantageous economics and current diffusion (IEA, 2019).

2.2 Hydrogen from water and electricity

A promising pathway to produce hydrogen in the future considers using the conversion of electricity, from renewable energy resources, towards chemical energy in an electrochemical process.

Electrolysis, more precisely water electrolysis, is the electrochemical process consisting in the separation of water into Hydrogen and Oxygen. The global chemical reaction of water electrolysis is written as follows:

$$H_2O \rightleftharpoons H_2 + \frac{1}{2}O_2 \qquad (2.5)$$
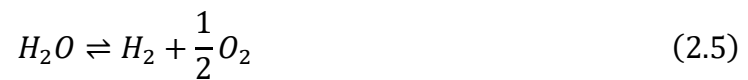
Concerning the physical structure of the reaction, it is performed in a unit called electrolyzer.

According to the description provided by (Coutanceau et al., 2018), The electrolyzer consists in two electrodes, anode and cathode, where the oxidation and reduction reaction progress, connected to an electric generator and divided by a ionic conductor, the electrolyte. The electrolyzer is variable in size: small, appliance-size equipment for local distributed production or large-scale for a centralized production system. The latter consists in direct connection to renewable or other sources of electricity that don't generate greenhouse gases. Today, the electrolyzers can operate with efficiencies of 60% to 80%, varying with the type of electrolyzer used and with the load factor.

Currently, the Hydrogen produced by means of water electrolysis counts, globally, less than 0.1% and (IEA, 2019). This technology is mostly used in markets that required Hydrogen with a high level of purity, e.g. electronics, polysilicon.

Also, in the process for producing chlorine and caustic soda Chlor-alkali electrolysis obtains as a by-product Hydrogen; this represents around 2% of total global production of H_2.

Even though, nowadays, the Hydrogen obtained by clean sources, called green Hydrogen, represents only a minor percentage to the overall production, the reduction in costs of electricity from renewable energy sources, (e.g. solar PV and wind), is causing an increase of share of the Hydrogen resulting from the electrolysis process.

It is important to consider that water electrolysis requires freshwater. According to IEA Greenhouse Gas R&D Programme IEAGHG Technical Review, this process requires 9 liters of water to obtain 1 kg of Hydrogen and 8 kg of oxygen, (useful for healthcare or industrial purposes)(IEAGHG, 2017a).This translates in 617 million cubic meters of water demand for covering the global production of hydrogen, 70 MtH_2.

There are three main technology options to realize the reaction: alkaline electrolysis cells (AEC), proton exchange membrane (PEM) electrolysis and

solid oxide electrolysis cells (SOEC), according to the ionic species that is transported through the electrolyte.

2.2.1   Alkaline Electrolysis (AEC)

Electrolyzers that use this technology are the most mature and commercially present. Since the first decades of the 20th century, especially fertilizer and chlorine industries have integrated this concept for the production of Hydrogen (X. Zhang et al., 2015).

In an Alkaline electrolysis cells, the ionic species transported are hydroxide ions (OH^-) from the cathodic side, where the Hydrogen is produced, to the anodic side passing via electrolyte. The electrolyte currently used in this device is a liquid alkaline solution of sodium or potassium hydroxide at a concentration of 25 to 30%, (David et al., 2019), in the main commercial product. However, a solid alkaline exchange membrane could be a promising future alternative as electrolyte.

The reactions involved at the two electrodes, respectively anode and cathode, are displayed:

Anode: $$2OH^-(aq) \rightarrow H_2O + 2e^- + \frac{1}{2}O_2(g)$$ (2.6)

Cathode: $$2H_2O\ (l) + 2e^- \rightarrow 2OH^-(aq) + H_2(g)$$ (2.7)
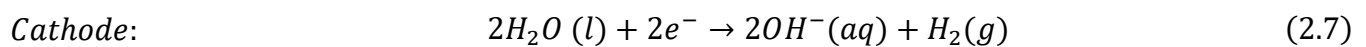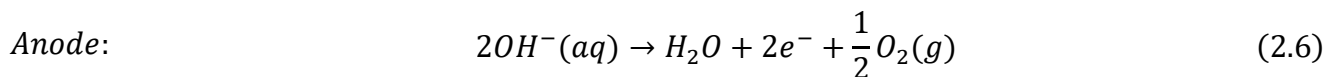
Alkaline Electrolyzers can operate from a minimum load of 10% to full design capacity. Before natural gas and steam methane reforming prevailed in the 1970s, Alkaline electrolysis was spread using large hydropower resources with capacities up to 165 MW$_e$ (IEA, 2020a).

The state-of-art AEC systems are easily available in the market. This technology can boast high durability, a system lifetime of 20-30 years, (Dincer & Acar, 2016), and the lowest capital cost among the water electrolyzers, avoiding the use of noble materials. Also, the stack components are already mature (Carmo et al., 2013; Zeng & Zhang, 2010).

However, this technology option presents some disadvantages concerning low current density, the high influence of the operating pressure with a negative impact on the system size and, considering the low efficiency, high Hydrogen production costs. Additionally, the device suffers low robustness, it is subjected to corrosion, high ohmic drop due to the liquid electrolyte and requires complicate maintenance requirements. In addition, the system requires 15 minutes for a cold start-up. This makes it unsuitable for fast response or varying power input, common in intermittent renewable sources (Dincer & Acar, 2016; Guo et al., 2019).

2.2.2 Proton Exchange Membrane or Polymer Electrolyte Membrane Electrolyzer (PEM)

This system was originally brought in the market at the beginning of the second half of the last century by General Electric to surmount some deficiencies of the alkaline electrolyzers (X. Zhang et al., 2015).

In PEMEC the electrolyte used is a solid plastic material or solid polymer electrolyte (SPE), commonly Nafion®. This perfluorinated polymer, containing sulphonic acid groups with high proton conductivity (0.1±0.02 S cm^{-1})(Slade et al., 2002), allows the exchange of protons (H$^+$), low gas crossover, compact system design and high pressure operation, as stated in Carmo et al., 2013.

Connected to the electrolyte, completing the sandwich strucure, known as MEA (membrane electrode assembly),there are the two eletrodes. The most common material for the cathodic catalyst layer is platinum, whereas for anodic side iridium is the most frequent,due to its better catalytic properties when used in the anode half-reaction.

At the anode, protons are released by means of the oxidation of water. Protons, then, flow through the membrane to reach the cathode where the reduction reaction occurs producing hydrogen, as displays in the following reaction:

$Anode$: $$H_2O(l) \rightarrow \frac{1}{2}O_2(g) + 2H^+(aq) + 2e^-$$ (2.8)

$Cathode$: $$2H^+(aq) + 2e^- \rightarrow H_2(g)$$ (2.9)
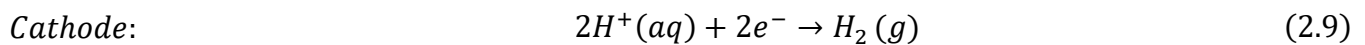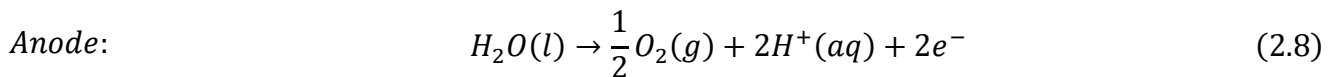
In the PEM, the use of pure water as the electrolyte solution allows to avoid the recovery and recycling of the potassium hydroxide required in the AEC solution. With respect to the alkaline, they are smaller and, thus, more suitable for urban applications in a decentralized production and for storages of highly compresses hydrogen (e.g. refueling stations).

Several other positive features are present in PEM electrolyzers. Thanks to the low permeability of Hydrogen through Nafion®, this technology can operate in a load range from 0% to 160% of design capacity, ensuring flexibility in operations (Barbir, 2005).

It can work at higher current density, above 2 A/cm^2, reducing the operational costs and, as a consequence, the overall electrolysis cost. The thinner electrolyte, with respect to alkaline cell, allows a lower value of ohmic losses. The fast flow of protons transported through the membrane, not delayed by the inertia of a liquid solution, allows a quick system

response to power input variations, with a cold-start time lower than 15 min, as reported by (David et al., 2019; Lehner et al., 2014).

According to the work of (Medina & Santarelli, 2010), using a solid electrolyte ensures compactness, strength and structural resistance, allowing to operate at high levels of pressure, up to 350 bar, as claimed by (Ayers et al., 2019).

High operating pressures in the electrolyzer generate high pressurized hydrogen. This is subject to electrochemical compression, allowing the final user to exploit less energy in the compression in the storing. Moreover, following the Fick's law of diffusion, in (Grigor'ev et al., 2001) it is highlighted how produced gas removal is improved considerably with the help of the reduced volume of the gaseous phase at the electrodes, due to the high pressure. The same study shows how the catalytic layer preserves its integrity thanks to a minimized expansion and dehydration of the membrane directly linked to the increase of pressure.

Even though it is the clear the amount of advantages, this technology must deal with some disadvantages.

Starting with high operational pressure, it can cause gas cross-permeation phenomenon, leading to the recombination and, thus, reduction in hydrogen yield as well as to chemical and structural degradation, better described in the further chapters.

PEM electrolyzers are still small-scale technology with stack currently below MW range, with a shorter lifetime with respect to alkaline electrolyzers and with high water purity requirements.

However, the main issue related to PEM concerns the cost of the materials of the component. Due to the corrosive acidic environment (pH∼2), consequence of the proton exchange membrane, and to the high applied over voltage, special, expensive, and mostly scarce materials and component must be selected.

These materials are for example noble metals for the catalyst (Platinum group metals- PGM, e.g. Pt, Ir and Ru), titanium-based metals for the current collectors and separator plates.

Among these elements, Iridium is present on Earth in a limited amount, with an average mass fraction of 0.001 ppm in the Earth's crustal layer; according to (Mitchell & Keays, 1981; Parry, 1984) it is 10 times less abundant than Platinum.

2.2.3   Solid Oxide Electrolyzer Cell (SOEC)

SOEC technology is the least mature electrolysis option. It is the youngest, not yet widely commercialized and still on the demonstration scale. However, it is clear the aim of some companies to introduce it in the market due to its high efficiency in production.

The electrolyte used in SOEC is a ion-conducting ceramics, such as Yttria stabilized Zirconia (Laguna-Bercero, 2012).These materials allow this technology to operate at high temperature, reason why SOECs are also known as High Temperature Electrolyzers (HTE) around 650-1000°C (A. Kilner, S.J. Skinner, 2012; Laguna-Bercero, 2012). This condition results in higher efficiencies compared to the alkaline and polymer membrane options.

Through the solid ceramic electrolyte, oxygen ions negatively charged (O^{2-}) are selectively conducted, generating Hydrogen at the cathode in a slightly different way with respect to AEC and PEM electrolyzers.

At the cathode, water combines with electrons flowing in the external circuit using the external generator. Here, Hydrogen in gas form is produced as well as negatively charged oxygen ions, following the reaction:

$$H_2O\ (g) + 2e^- \rightarrow O^{2-} + H_2(g) \tag{2.10}$$
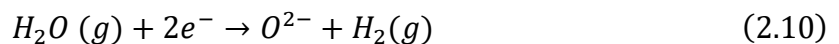
When the oxygen ions cross the solid ceramic membrane reaching the anode, the oxidation reaction occurs generating as product oxygen in gas phase and electrons that enter the external circuit. On this electrode the reaction is as follows:

$$O^{2-} \rightarrow \frac{1}{2}O_2\ (g) + 2e^- \tag{2.11}$$
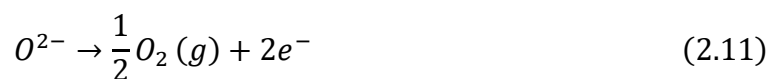
Even though they are still at laboratory scale, SOECs have already displayed their high potential in terms of high degree of electrical efficiencies (up to 110%, according to the analysis of (Lehner et al., 2014)). Indeed, working at high temperatures allows to reduce the electrical requirements, with the possibility of using waste heat (Badwal et al., 2013). The YSZ ceramic electrolyte, the electrodes, Nickel based cathode and Perovskite-type lanthanum strontium manganese anode, can be purchased at low cost, especially with respect to PEM electrolyzers.

Interesting characteristic about this new option is the possibility to work in a reverse mode, as a fuel cell, converting Hydrogen back to electricity, in this way it can ensure a balanced grid if combined with Hydrogen storage facilities and guarantee a higher overall utilization rate of the system.

Another positive aspect is linked to the high tolerance to carbon molecule. This property allows SOECs to operate in co-electrolysis mode: through the utilization of water stream (H_2O) and carbon dioxide in the reaction, it is possible to produce a gas mixture (carbon monoxide and hydrogen), named syngas, converted in a second step in synthetic fuel (A. Kilner, S.J. Skinner, 2012; Xu et al., 2016).

In addition, it is important to consider among the advantages that the solid structure of SOEC and PEM technology results in mechanical and chemical stability, robustness and compactness.

However, still some challenges must be faced by SOEC electrolyzers. The severe material degradation mainly related to the operation at high temperatures still defies its durability. Therefore, researches are currently focused on developing new component materials or working on existing ones which can withstand the high operating temperature. Scientist are also working on keeping the high efficiency at lower temperatures in the range of 500-700°C to boost its commercialization (Laguna-Bercero, 2012; Lehner et al., 2014).

2.3 Hydrogen from Coal

Coal represents a well-known source for the production of hydrogen. The hydrogen obtained from this fossil fuel is called brown hydrogen and counts for the 23% of total Hydrogen produced in 2018 according to (Proost, 2020), mostly in China. The main process involving coal in this field is the gasification, although, some new projects involving high-pressure partial oxidation using lignite are currently in operation (*Latrobe Valley | Hydrogen Energy Supply Chain*, n.d.).

Like natural gas, involving hydrocarbons in the process generates CO_2 emissions. In the gasification reaction of coal the rate is about 19 tCO_2/tH_2, twice the emission ratio obtained by the reactions with natural gas, (Steam Methane reforming emits 8 tons of CO_2 per ton of H_2 produced (IEA, 2019, 2020a). As a result, the spread of this technology is intrinsically linked to the evolution of Carbon Captures technologies.

2.3.1   Coal Gasification

The reaction, through the solid fuel gasification of coal, produces the mixture of hydrogen and carbon monoxide, i.e. syngas.

The reaction happens between oxygen, steam, and the carbon molecule present in coal, occurring at high temperature and pressures. Following are the main reactions involved in the process:

$$C + H_2O \rightleftharpoons CO + H_2 \quad \Delta H_{rx} = 131 \frac{kJ}{mol} \tag{2.12}$$

$$C + O_2 \rightleftharpoons CO_2 \quad \Delta H_{rx} = -394 \frac{kJ}{mol} \tag{2.13}$$

$$C + \frac{1}{2}O_2 \rightleftharpoons CO \quad \Delta H_{rx} = -111 \frac{kJ}{mol} \tag{2.14}$$

$$C + CO_2 \rightleftharpoons 2CO \quad \Delta H_{rx} = 172 \frac{kJ}{mol} \tag{2.15}$$
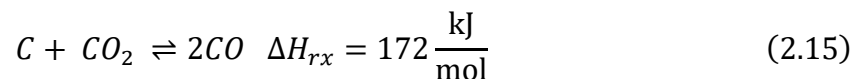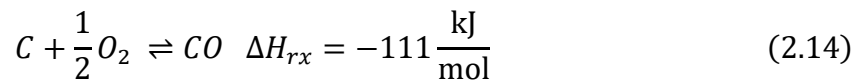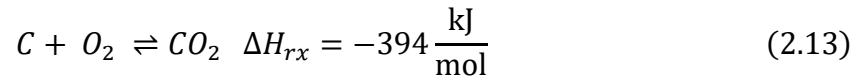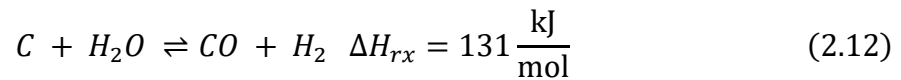
Currently, the most common gasifier in the market is the entrained-flow gasifier; well-established examples are provided by GE and Shell Gasifiers. The first one produces the gasification at operating temperatures varying between 1300°C-1500°C and at pressures up to 100 bar, depending on the type of gas required as final product (85-100 bar for ammonia, 60-70 for methanol). Instead, in the second one typical pressures are about 20-40 bars and temperatures range of 1400 °C-1600°C (Ke Liu, Cui, et al., 2009).

In the same way as for reforming process, after the production of syngas from gasification, the mixture is involved in the "water-gas-shift" reaction, described in the equation (2.2), in order to further increase the Hydrogen generation.

2.4 Hydrogen from biomass

Another main pathway for the hydrogen production starts from biomass. Biomass can be treated in different ways: biochemically, exploiting microorganisms' action on organic material through anaerobic digestion process which results in the creation of biogas or by means of a fermentation process obtaining a combination of acids, alcohols and gases.

Beside these processes, biomass can be exploited in a thermochemical gasification. The working principle is the same of coal gasification, explained in the chapter 2.3.1, converting the biomass source into CO, carbon dioxide, hydrogen and methane.

From a technical point of view, the most well-established technology exploits the process of anaerobic digestion to produce biogas. However,

only sewage sludge, food processing, agricultural, energy crops and household waste can be processed in this process. The non-edible cellulose-based components present in some plants can be involved in the fermentation process.

In general, all organic materials, especially the lignin component in biomass, can be gasified. Gasification, however, is not fully developed, despite some demonstration plants around the world (Hrbek, 2015). From these plants it is still clear the issues related to the formation of tars, dangerous for the catalyst (Ericsson, 2017).

In the same way of coal gasification and reforming technology, the products have to be further treated to obtain hydrogen, increasing the already high complexity of the biomass processes directly related to a higher cost of production of low-carbon hydrogen than electrolyzers supplied by a renewable energy source (solar or wind).

Beside the complexity, the limited amount of available cheap biomass still hinders the diffusion of large-scale hydrogen production from biomass.

However, this technology still remains an option considering a combined operation with carbon capture and storage in terms of "negative emissions"(IEA, 2019).

2.5 Technologies comparison

After the analysis of the technologies currently diffused in the Hydrogen field, it is useful to highlight the key points for a comparison and eventually for the selection of the technology.

The parameters chosen for the analysis are cost of production and carbon intensity.

2.5.1   Cost

Researchers and companies are working towards a reduction of capital cost of electrolyzers to make Hydrogen produced by renewable electricity, i.e. green hydrogen, cost competitive with Hydrogen produce by fossil fuels.

Nowadays, the cost of producing Hydrogen from natural gas without carbon capture utilization and storage (CCUS) technologies is in the range 1-2 USD/kgH$_2$ highly dependent on the fuel costs, between 45% and 75% of the cost, variable in time and more significantly among the different regions

of production (IEA, 2019). With CCUS the range goes between 1.4 and 2.4 USD/kgH$_2$, positioning this option as the cheapest low-carbon technology (IEAGHG, 2017b).

Apart from Hydrogen obtained from coal, where CAPEX has the main percentage, 50%, fuel costs cover the biggest share in the production cost. Therefore, the price of electricity and gas and related factors, for instance conversion efficiencies (figure 2.2) are heavily relevant.

Electrolysis cost is defined also by the CAPEX requirements and the annual operating hours. Today electrolysis CAPEX range, mainly due to the stack cost, varies according to the type of technology: 500–1400 USD/kW$_e$ for alkaline, 1100–1 800 USD/kW$_e$ for PEM electrolyzers, 2 800–5600 USD/kW$_e$ estimation for SOEC electrolyzers. Clearly, an increase in the operating hours will allow a lower impact of CAPEX in the total cost, increasing the dependence on electricity price (Proost, 2018).
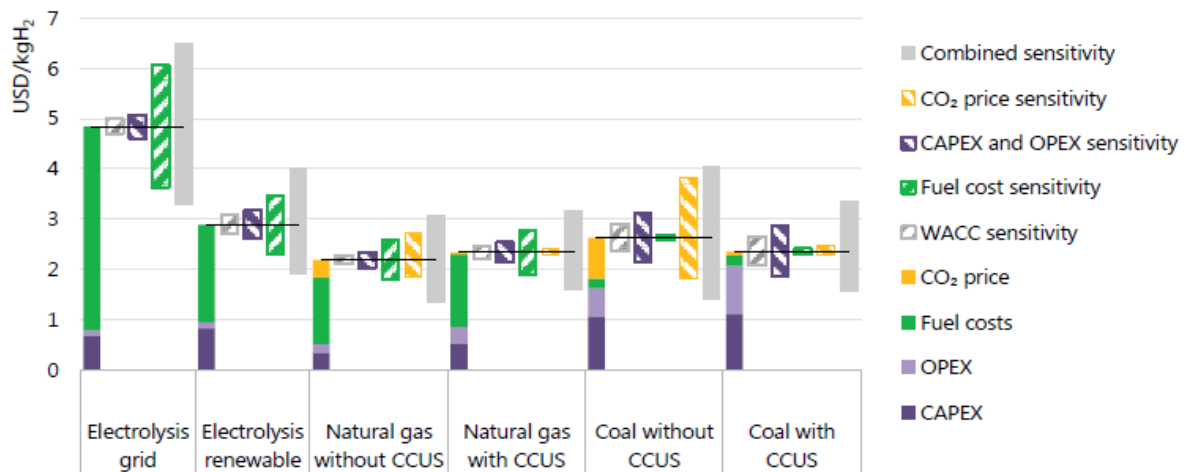
Notes: WACC = weighted average cost of capital. Assumptions refer to Europe in 2030. Renewable electricity price = USD 40/MWh at 4 000 full load hours at best locations; sensitivity analysis based on +/-30% variation in CAPEX, OPEX and fuel costs; +/-3% change in default WACC of 8% and a variation in default CO$_2$ price of USD 40/tCO$_2$ to USD 0/tCO$_2$ and USD 100/tCO$_2$. More information on the underlying assumptions is available at www.iea.org/hydrogen2019.

Source: IEA 2019.

Figure 2-2 Hydrogen production costs for different technology options, 2030 (IEA, 2019)

From the figure 2-2, it is shown that electrolysis is not cost competitive with respect to fossil fuels options, but innovation, using less costly materials, economies of scale in the manufacturing processes will influence considerably the cost. In particular, it is possible to increase the total capacity of the electrolyzers combining them in a multi-stack configuration.

Finally, IEA reports that electrolyzers could represent a low-cost option for hydrogen supply at location with optimal renewable resource due to the decreasing costs of the renewable, i.e. for solar PV and wind generation,

even considering the transmission and distribution costs of transporting hydrogen from (often remote) renewables locations to the final users (IEA, 2019).

2.5.2   Carbon intensity

Even though from the cost analysis it appears that fossil fuels still prevail in the next future Hydrogen market, the assessment of the different technologies must be carried on considering the second parameter in the comparison. Indeed, the amount of CO_2 emissions produced which covers a significant range depending on the fuel and technology involved.

Firstly, coal represents the main cause in CO_2 generation amid the considered technologies. The ratio $kgCO_2/kgH_2$ resulting from all the Hydrogen production pathways involving this fuel, without carbon capture devices, is higher than 20 $kgCO_2/kgH_2$. Using the electricity from coal-fired generation in the electrolysis process emits almost 40 kg of carbon dioxide per 1 kg of hydrogen produced, making this option the worst in terms of CO_2 intensity.

Although with a lower carbon footprint with respect to coal, almost half, natural gas is the second source concerning emission levels.

As for the hard coal, it is less carbon intense to produce Hydrogen directly from reforming processes of natural gas than using it in a gas-fired generator of electricity, and consequent electrolysis. The latter has a ratio between CO_2 emitted and H_2 produced greater than 15 $kgCO_2/kgH_2$, whereas the option of natural gas without CCUS is responsible for less than 10 kg of carbon dioxide for the same amount of Hydrogen obtained.

Considering that, according to the Statistical Review of World Energy analyses provided by BP (BP, 2020), in 2020 63,3% of overall electricity has been produced by fossil fuels, the emissions resulted by an electrolysis using world average electricity mix exceed 25 kg of CO_2.

Taking into account only the direct carbon dioxide emissions at the electricity generation plant, renewable energy sources and nuclear generation represent the best option, allowing to exploit electrolysis with the ratio emission over production equal to 0 $kgCO_2/kgH_2$ (IEA, 2019).

2.5.3   Conclusions

From the discussion above, it is possible to conclude that currently the Steam Methane Reforming of natural gas with CCUS seems to be the most convenient considering the combination of cost and carbon intensity.

However, the decreasing of costs for solar PV and wind generation is becoming clear, allowing to consider the electrolysis exploiting the renewables or nuclear power as a low-cost and low carbon intense supply option for Hydrogen production, taking into account the cost for transmission and distribution in case of remote renewables locations.

In any case, the key to make the renewable water electrolysis cost-competitive is linked to higher carbon taxes imposition, already in the near future policies of several countries (Environment, 2021; European Commission, 2019); action that directly influence the cost of Hydrogen, as a parallel action to researches in better and cheaper technologies (Hydrogen Europe, 2019; Nikolaidis & Poullikkas, 2017).

According to this promising premise and to the wide knowledge gap, it has been chosen to analyze the water electrolysis and, in particular, considering efficiency, flexibility to renewables sources and level of development of the technology. The Proton Exchange membrane water electrolyzers represents currently the most promising for the near future in the contest of CEE. Simplicity, excellent dynamic response to power fluctuation, possibility of compact design are just some of the advantages making PEM the ideal technology among the other available electrolyzer for operation with intermittent wind and solar power (Chandesris et al., 2015; Schmidt et al., 2017).

3 PEM water electrolyzer modeling

3.1 Electrochemical Model

This chapter is focused on the modeling of PEM electrolyzer.

The thermodynamic principle behind the operation of the Proton Exchange Membrane electrolyzer is shown in figure 3-1 and explained in the partial reactions of Eqs. (2.8) and (2.9). A direct electric current provided by a power supply leads to the decomposition of water, driving the generation of O_2 and protons H^+. The hydrogen ions move through the polymeric membrane by means of the voltage gradient from the anode to the cathode where they are recombined with the electrons flowing in the external circuit to produce hydrogen.
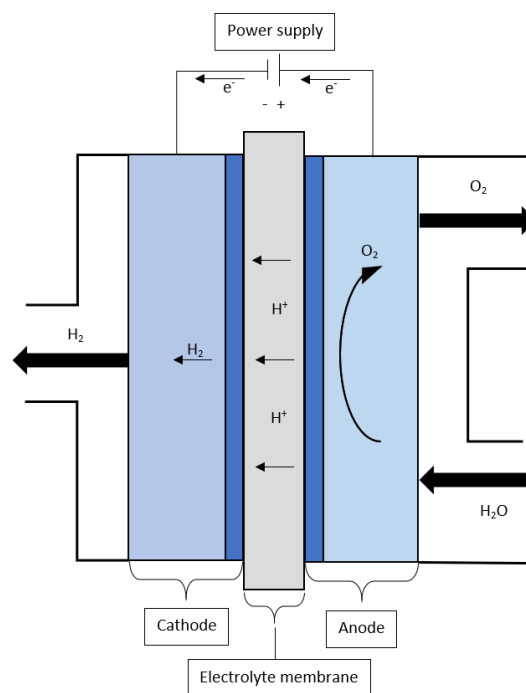
Figure 3-1 Simplified model of PEMWE
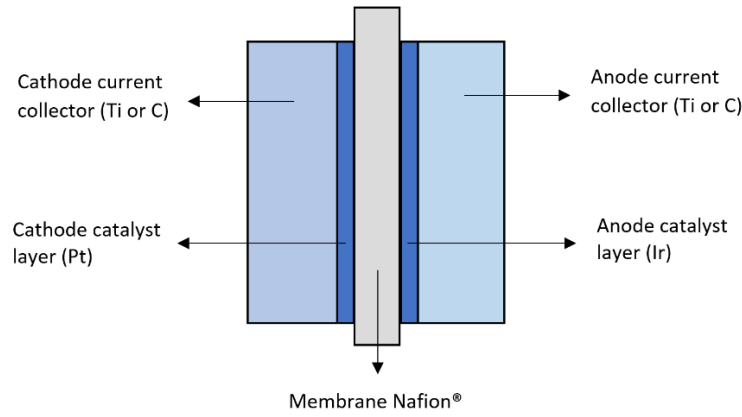
Figure 3-2 Focus on MEA[1] structure

The electrolysis process is naturally not spontaneous. Thus, the conversion from electrical energy to chemical energy through the electrochemical reaction is possible only if the electromotive force provided by the supply, and, consequently, the voltage gradient generated are sufficiently high to cover at least the ideal voltage at open circuit conditions, directly related to the Gibbs Free Energy of the process. In real operation, the voltage required is higher because of the non-faradaic losses involved in it. These losses determine an activation overvoltage, $V_{act,EL}$, an ohmic overvoltage, $V_{ohmic,EL}$, and concentration overvoltage, $V_{conc,EL}$. The mass transport, the resistance to the flow of protons in the electrolyte membrane and the electric current in the cell components are the main cause of the listed overvoltages (Bessarabov & Millet, 2018). The voltage gradient between anode and cathode is, thus, given by:

$$V_{EL} = V_{OC,EL} + V_{act,EL} + V_{ohmic,EL} + V_{conc,EL} \qquad (3.1)$$

In the next section, the mathematical models of these voltage terms are explained in detail.

3.1.1   Electrolyzer Open Circuit Voltage $V_{OC,EL}$

With the expression *Open Circuit Voltage, OCV,* it is defined the voltage corresponding to null current operating conditions, resulting in absence of losses. According to (Abdin et al., 2015; Görgün, 2006), $V_{OC,EL}$ depends on the reaction electrochemistry with a correction on the pressure. It can be described by the Nernst Equation, reported as follows:

$$V_{OC,EL} = E_{Nernst} = E^0 + \frac{RT}{nF}\ln\left(\frac{a_{H_2}a_{O_2}^{\frac{1}{2}}}{a_{H_2O}}\right) \qquad (3.2)$$

---

[1] MEA=Membrane Electrode Assembly.

Here, a_{H_2}, a_{O_2} and a_{H_2O} indicate the chemical activities at the catalyst layers respectively of Hydrogen, oxygen and water between electrode and membrane (1 for liquid water) with their respective stoichiometric factors. R is the universal gas constant (8.314 J/(mol*K)), T is the cell temperature, n is the stoichiometric coefficient corresponding to the number of electrons moles per Hydrogen moles involved in the reaction, here 2, F is the Faraday's constant (96485 C/mol). E^0 is the standard potential or reversible voltage calculated from the Gibbs free energy:

$$E^0 = \frac{\Delta \hat{g}^0(T, p_{ref})}{nF} \tag{3.3}$$

$\Delta \hat{g}^0$ is the Gibbs free energy of the reaction of hydrolysis (Eq. 2.5) in standard conditions (1 atm pressure).

Activities are difficult to define, therefore, the equation (3.1) is often simplified, assuming the ideal gas behavior. Likewise in (Colbertaldo et al., 2017; Larminie & Dicks, 2003), instead of the activities, the partial pressures of the Hydrogen and oxygen and the saturation pressure of water at the operating temperature are involved as follows:

$$V_{OC,EL} = \frac{\Delta \hat{g}^0(T, p_{ref})}{nF} + \frac{RT}{nF} \ln\left(\frac{p_{H_2} p_{O_2}^{\frac{1}{2}}}{p_{H_2O}} \right) \tag{3.4}$$

The value of the reversible cell voltage is commonly assumed equal to 1.23 V by many authors. However, this result is valid only at standard temperature and pressure. As pointed in the study of (Awasthi et al., 2011), E^0 is dependent on operating temperature of the cell:

$$E^0 = 1.229 - 0.9 * 10^{-3} * (T_{el} - 298) \tag{3.5}$$

Adopting the approach used in (Biaku et al., 2008), it is assumed that the pressure applied by the water in liquid form is equivalent to the saturation pressure of vapor, P_{sat,H_2O}, and that oxygen and Hydrogen are the only gas present respectively at the anode and cathode. Considering that low pressures are involved in the process, Dalton's law of partial pressures can be used. The three pressures are, then, obtained as follows:

$$P_{sat,H_2O} = 610 * 10^{-5} * e^{\left[\frac{T_c}{T_c + 238.3} * 17.2694 \right]} \tag{3.6}$$

$$p_{O_2} = P_{anode} - P_{sat,H2O} \tag{3.7}$$

$$p_{H_2} = P_{Cathode} - P_{sat,H2O} \tag{3.8}$$

The temperature T_c introduced in (3.5) is given in Celsius (°C), while P_{anode} and $P_{cathode}$ refer to the total pressures at the two electrodes. Next, the description of the models for overpotentials is given.

3.1.2   Overpotentials

Before the actual production of hydrogen and oxygen can occur, some irreversibilities present in the system require a higher potential to be overcome. These overpotentials are mainly the activation and the ohmic, and, in minor share, because of the low operating current density, the concentration overpotential (Biaku et al., 2008).

3.1.2.1 Activation overvoltage $V_{act,EL}$

The first loss to be analyzed is the one responsible of the activation overpotential. This voltage increment hinges on the kinetics of the reactions occurring in the catalyst layer in the anodic and cathodic interface with the electrolyte. On the interface, the formation of an electrical double layer (EDL) takes place by means of the protons produced at the electrode, migrated in the solution and accumulated on the interface. Because of the presence of the electrical double layer, a capacitive behavior occurs at the electrode, opposing the electric field, a resistance to the charge and mass transfer. At last, this phenomenon results in a higher voltage to apply.

As pointed in (Carmo et al., 2013; García-Valverde et al., 2012), several parameters are involved in the modelling of this phenomenon, increasing its complexity and difficulty. It assumes a certain relevance the manufacturing in the material processing; the morphology and active catalyst area can cause flow restrictions at the catalyst sites as well as temperature, pressure, utilization, distribution and age.

Following the common approach used in (Abdin et al., 2015; Colbertaldo et al., 2017; García-Valverde et al., 2012), the activation overpotential can be described, both for the anode and the cathode by the Butler-Volmer (B-V) expression, reported as follows:

$$V_{act,EL} = \frac{RT}{\alpha_{an}F}\sinh^{-1}\left(\frac{i}{2i_{0,an}}\right) + \frac{RT}{\alpha_{cat}F}\sinh^{-1}\left(\frac{i}{2i_{0,cat}}\right) \tag{3.9}$$

Where α is the dimensionless charge transfer coefficient respectively at the anode and at the cathode, F is the Faraday constant, R is the universal gas constant, T is the temperature, i is the current density, whereas i_0 represents the exchange current density at the electrodes. The value of α for the two electrodes is reported differently in some literature. In (Carmo et al., 2013), for example, the values assumed are α_{an}=2 and α_{cat}=0.5. (Awasthi et al., 2011; Biaku et al., 2008), instead, take into consideration

that the Butler-Volmer equation is obtained with the assumption of symmetry of the reactions at the electrodes of oxidation and reduction. As a consequence, they consider the same value for the two transfer coefficients. This single value can vary from 0.18 to 0.42, even if often assumed equal to 0.5 (Abdin et al., 2015; Colbertaldo et al., 2017; García-Valverde et al., 2012).

In any case, the most variable parameter of this equation among literature is the i_0, with a range of variability that cover seven order of magnitude (10^{-13}–10^{-6} A/cm^2, (Marangio et al., 2009)).

The value of the exchange current densities depends on many physical parameters of the electrocatalyst and electrodes (mainly materials, dimensions, temperature, pressure).

In general, the exchange current density is modelled focusing on the temperature dependence by means of Arrhenius-based equation, reporting (Liso et al., 2018), as follows:

$$i_0 = \gamma_M i_{o,ref} * e^{\left[-\frac{E_a}{R}\left(\frac{1}{T}-\frac{1}{T_{ref}}\right)\right]}$$
(3.10)

Here, γ_M is the roughness factor: portion of geometric area of the MEA electrochemically active. This parameter is proportional to the catalysts' properties: density (IrO$_2$ and Pt), leading, crystallite diameter and the percentage of metal surface of the catalyst in contact with the ionomer.

In the Eq. (3.10), $i_{o,ref}$ is the exchange current density at the reference temperature, T_{ref}, empirically obtained. E_a indicates the activation energy for the electrode reaction.

In the model, the values, assumed by (Liso et al., 2018) and shown in Table 1, are considered.

Table 3-1 Fixed model parameters

Parameter		
T_{ref}	298 K	
	Anode	**Cathode**
γ_M	$7.23 * 10^2$ cm^2/cm^2	$2.33 * 10^2$ cm^2/cm^2
$i_{o,ref}$	$5 * 10^{-12}$ A/cm^2	$1 * 10^{-3}$ A/cm^2
E_a	76 kJ/mol	4.3 kJ/mol

3.1.2.2 Ohmic overpotential $V_{ohm,EL}$

The second loss with a considerable effect is the ohmic overpotential. The phenomenon behind this irreversibility consists in the electrical resistances

encountered by the electrons' movement in the different parts of the cell (electrodes, GDL, bipolar plates, channels) and, mainly, by the protons moving in the membrane. As explained in (Colbertaldo et al., 2017), the mechanism can be described by the Ohm's law:

$$V_{ohm,EL} = R_{ohmic,tot} * I \qquad (3.11)$$

In the Eq. (3.10) the I is the cell current, while $R_{ohmic,tot}$ is the total resistance computed as the sum of the resistances in the electrode and the membrane, as follows:

$$R_{ohmic,tot} = R_{el} + R_{mem} \qquad (3.12)$$

In the literature, (García-Valverde et al., 2012; Liso et al., 2018), the current density i is considered as:

$$i = \frac{I}{A} \qquad (3.13)$$

we can write the Eq. (3.10) as follows:

$$V_{ohm,EL} = (r_{el} + r_{mem}) * i \qquad (3.14)$$

Here, r_{el} and r_{mem}, $[\Omega * cm^2]$ are called Area Specific ohmic Resistances (*ASR*) defined for a specific cell. The value r_{el} can be obtained measuring the resistance between the stack terminals at open circuit condition. Although, as reported in the study of (X. Li, 2005), the irreversibilities occur mainly in the membrane, for this reason, the equation (3.14) is simplified involving only the area specific resistance of the membrane, r_{mem}.

Considering that ASR is indipependent on the current density, the ohmic overpotential follows a linear behaviour with respect to i. Instead, the resistance is strongly interconnected with the membrane conductivity, σ_{mem}, as well as with the membrane thickness t_{mem}, that the protons have to cross. The relationship is reported as follows:

$$r_{mem} = \frac{t_{mem}}{\sigma_{mem}} \qquad (3.15)$$

Several studies have been carried out for the evaluation of the membrane proton conductivity, σ_{mem}. The main models used in the literature are derived from the work of (Kopitzke et al., 2000) that focuses on the temperature, or from (Springer et al., 1991), where the connection with the water content is also considered. A third model is explained in (Bernardi & Verbrugge, 1991), where a more detailed analysis is carried out involving the diffusion coefficient and the bulk concentration of protons. The model adopted in this work is the most common empirical relation discussed in

(Springer et al., 1991) and (Carmo et al., 2013; Santarelli et al., 2006), reported as follows:

$$\sigma_{mem} = (0.005139 * \lambda - 0.00326) * e^{\left[1268*\left(\frac{1}{303} - \frac{1}{T_{avg}}\right)\right]}$$

(3.16)

Here, the variable λ represents the degree of hydration of the Nafion membrane $[\text{mol}_{H_2O}/\text{mol}_{SO_3^-}]$. Many studies have tried to model the variation of the water uptake. However, in the case of PEM water electrolyzer, considering the large amount of water sent in the anode intake, it is reasonable to assume a fully hydratation of the Nafion membrane (Marangio et al., 2009). The range in which λ varies goes from 14 to 21. According to the mention assumption, we consider 20 as the value of λ for modelling purposes (Awasthi et al., 2011).

If the activation losses prevail at low current densities, the voltage increase related to ohmic overpotential is dominant for higher currents densities where the higher production is experienced. For this reason the operational point has to be a trade-off between production and losses.

3.1.2.3 Concentration overpotential $V_{conc,EL}$
The concentration or mass transport overpotential are the result of the concentration variation of the reactants occurring at the interface with the electrodes during the electrolysis. A high current is able, indeed, to alter the rate of the reaction at the catalyst layer. In particular, gas bubbles are generated in these conditions, causing a limitation in mass transport and, thus, a reduction in the reaction kinetics. Due to the larger volume of the oxygen bubbles produced, the main contribution is given by the anodic side, which is, therefore, the only share considered in the modelling (García-Valverde et al., 2012).

The parameters involved in the modelling are the current, the reactant activity and the electrode structure. The analytical expression commonly used in literature, as shown in (Carmo et al., 2013), consists in a relationship connecting this overpotential to the temperature and to the concentration, the latter both in bulk phase and in the reaction phase. However, it is common to involve the dependence on the concentration in the parameter called limiting current density, i_L. This variable is defined by (Selman & Tobias, 1978) as "maximum rate at 100% current efficiency, at which a particular electrode reaction can proceed in the steady state", or the current density at which the concentration of the reactants tends to zero. In the literature, the value assumed for i_L is $6\frac{A}{cm^2}$ (Bernardi & Verbrugge, 1991; García-Valverde et al., 2012). The general equation of the overpotential is presented as follows:

$$V_{conc,EL} = \frac{RT}{\alpha_{an}nF} \ln\left(\frac{i_L}{i_L - i_{an}}\right) \qquad (3.17)$$

The term *diffusion* overpotential is often used to define this class of irreversibility, focusing the analysis of the causes on the concentration gradient of charge-carriers between the electrolyte and the electrode. The mechanism is described in better details in (Marangio et al., 2009) .

It has been experimentally displayed that the share of this overpotential is significantly smaller than the activation and the ohmic terms, especially at low current densities. Commercial PEM electrolyzers, nowadays, operate at current densities insufficiently high to be affected by mass-transport limitation. Therefore, the concentration contribution is often neglected in these operating conditions (Carmo et al., 2013; Lebbal & Lecoeuche, 2009). In any case, from the equation (3.17), it is possible to see that at larger current densities, its contribution is increasingly significant.

3.2 Material Balance

The following section explains the mass balance of each species involved in the reactions, to understand the production rate of the Hydrogen in relation to the water consumption and oxygen production.

The production and consumption rate of the two gases can be described by the Faraday's Law:

$$\dot{N}_{species} = \frac{I}{nF} \qquad (3.18)$$

Where n is the number of moles generated or consumed for each electron.

3.2.1   Anode chamber

In the anodic side, the oxidation reaction of the oxygen involves four moles of oxygen per electron and, in parallel, two moles of water. The molar flows, respectively generated and consumed, are then defined as:

$$\dot{N}_{O_2}^{gen} = \frac{I}{4F} \qquad (3.19)$$

$$\dot{N}_{H_2O}^{cons} = \frac{I}{2F} \qquad (3.20)$$

It is common, with the same approach adopted for the Eq (3.13), to rewrite the current I as a function of cell area A and current density i.

As explained by (Abdin et al., 2015), the molar flow balance of oxygen can be written considering the difference between the entering and exiting fluxes. Then, to this balance it is added the amount of oxygen produced by the oxidation and deduced the quantity lost in cross penetration:

$$\frac{dN_{an,O_2}}{dt} = \dot{N}_{an,O_2}^{in} - \dot{N}_{an,O_2}^{out} + \dot{N}_{O_2}^{gen} - \dot{N}_{O_2}^{perm} \tag{3.21}$$

In the electrolyzer operation the only inlet flow is the water flow. Therefore, it is possible to assume a null value for the inlet contribution $\dot{N}_{an,O_2}^{in}$.

The term $\dot{N}_{O_2}^{perm}$ is used to compute the amount of oxygen that permeates the polymeric membrane: the oxygen dissolved in the water is carried by the water flow that cross over the Nafion®. According to (Ursúa et al., 2012), the flux is driven by the pressure gradient present between anode and cathode. Even if the percentage of flux led by pressure difference is secondary with respect to the other contributions, its presence is still significant concerning the safety in operation as well as the degradation of the cell. The safety issue, as reported by (Bessarabov et al., 2016), is connected to the high flammability of the mixture $H_2 - O_2$. Many studies, by (Chandesris et al., 2015), have pointed out how gas crossover, and the consequent Hydrogen peroxide production, lead to a faster degradation of the electrolyzer, as described in 3.4.

Likewise, the variation of water is computed subtracting to the water inlet flow the water exiting and consumed in the reaction and the contribution of the water crossing the membrane. (Abdin et al., 2015) reports as follows:

$$\frac{dN_{an,H_2O}}{dt} = \dot{N}_{an,H_2O}^{in} - \dot{N}_{an,H_2O,l}^{out} - \dot{N}_{H_2O}^{cons} - \dot{N}_{H_2O}^{mem} \tag{3.22}$$

Similarly, for the oxygen, gas crossover can occur for the Hydrogen molecules, although negligible. Because of this phenomenon, H$_2$ balance is defined at the anode as follows:

$$\frac{dN_{an,H_2}}{dt} = \dot{N}_{H_2}^{perm} - \dot{N}_{an,H_2}^{out} \tag{3.23}$$

3.2.2   Cathode chamber

A similar modelling approach is applied on the cathodic side. Here, the reduction reaction of the protons generates Hydrogen. The accumulation of H_2 is obtained by the addition of the generated contribution to the net molar flow:

$$\frac{dN_{cat,H_2}}{dt} = \dot{N}_{cat,H_2}^{in} - \dot{N}_{cat,H_2}^{out} + \dot{N}_{H_2}^{gen} - \dot{N}_{H_2}^{perm} \tag{3.24}$$

$$\frac{dN_{cat,H_2O}}{dt} = \dot{N}^{in}_{cat,H_2O} - \dot{N}^{out}_{cat,H_2O} - \dot{N}^{mem}_{H_2O} \qquad (3.25)$$

$$\frac{dN_{cat,O_2}}{dt} = \dot{N}^{perm}_{O_2} - \dot{N}^{out}_{cat,O_2} \qquad (3.26)$$

The generation is computed with the Faraday's law:

$$\dot{N}^{gen}_{H_2} = \frac{I}{2F} \qquad (3.27)$$

Due to the assumption of only water as inlet flow, also for Hydrogen $\dot{N}^{in}_{cat,H_2}$ is considered equal to zero. In addition, the contribution $\dot{N}^{cons}_{H_2O}$ is not present in the equation (3.25): the water consumption occurs only on the anode.

3.2.3   Membrane

Special attention must be given to the water transport and to the membrane contribution. Even though the design of the membrane has been chosen to be permeable only to protons, water diffusion across it occurs.

The process can be explained by the combination of three main phenomena: electro-osmotic drag, diffusion and hydraulic pressure effect reported in (Abdin et al., 2015).

$$\dot{N}^{mem}_{H_2O} = \dot{N}^{eod}_{H_2O} + N^{diff}_{H_2O} - \dot{N}^{pe}_{H_2O} \qquad (3.28)$$

The electro-osmotic drag term $\dot{N}^{eod}_{H_2O}$ defines the water dragged by the positive ions of Hydrogen in the membrane, the diffusion term $\dot{N}^{diff}_{H_2O}$ describes the transport mechanism caused by the concentration asymmetries. At last, also the presence of a pressures gradient between the two electrodes is responsible in the transport phenomena, which contribution is considered in the hydraulic pressure term $\dot{N}^{pe}_{H_2O}$. Next, each of these terms are explained in detail.

- Electro-osmotic drag $\dot{N}^{eod}_{H_2O}$

The mechanism of electro-osmotic drag, analyzed by (Springer et al., 1991), represents the most relevant in water transport. Part of the water is forced to flow from the anode to the cathode by the flux of the migrated hydrated protons. As reported by (Liso et al., 2018), the number of moles of water molecule dragged by each mole of H^+ is proportional to the ratio of the current applied I over the Faraday's constant F:

$$\dot{N}^{eod}_{H_2O} = n_d \frac{I}{F} \qquad (3.29)$$

Here, $n_d \, [mol_{H_2O} \, /mol_{H^+}]$, named osmotic drag coefficient, is defined as the number of water molecules dragged by each hydrogen ion. The literature is not uniform in setting the value of this coefficient: an experimentally obtained fixed value, (Awasthi et al., 2011), or correlated with the cathode pressure, operation temperature and current density, (Medina & Santarelli, 2010), or with the membrane humidification, (Dutta et al., 2001; Görgün, 2006).

In addition, according to (Onda et al., 2002), with a membrane in full hydration, with fix λ_m, the electro-osmotic coefficient can be obtained just with the temperature.

- Water diffusion $\dot{N}_{H_2O}^{diff}$

At the anode and cathode, the concentration of water is different. The gradient present, thus, induces the movement of water from one electrode at high concentration, anode, to one at low concentration, cathode. Being a diffusion phenomenon, the mechanism can be model by integration of the Fick's Law of diffusion between the two ends of the membrane, considered as interfaces, assuming a linear gradient (Abdin et al., 2015; Marangio et al., 2009; Medina & Santarelli, 2010).

$$\dot{N}_{H_2O}^{diff} = \frac{D_{H_2O}A}{t_{mem}}\left(C_{H_2O,mem,cat} - C_{H_2O,mem,an}\right) \tag{3.30}$$

Here, D_{H_2O} is the membrane water diffusion coefficient, t_{mem} is the thickness of membrane, A is the active area of the membrane whereas $C_{H_2O,mem,cat}$, $C_{H_2O,mem,an}$ are the water concentration at the interfaces with respectively the cathode and the anode.

The diffusion coefficient, D_{H_2O}, is, in literature, defined or as fixed, or function of degree of hydration, temperature and porosity.

The first case refers to the work of (Awasthi et al., 2011; Görgün, 2006) and (Abdin et al., 2015; Kim et al., 2013), in which the suggested values are respectively $1.25 * 10^{-10} \frac{m^2}{s}$ and $1.28 * 10^{-10} \frac{m^2}{s}$. The dependence on the temperature and porosity ε is, instead, considered by (Lin et al., 2004; Medina & Santarelli, 2010)

To compute the concentrations at the interfaces between membrane and electrodes, a linear diffusion behavior is assumed in the Gas Diffusion Layer (GDL).Here, the Fick's law is applied relating the concentrations to the thickness of the anode and the cathode GDL and to the effective diffusivity. This parameter is defined proportional to the binary diffusivity between each

gas and water corrected by a porous-dependent factor, as shown by (Santarelli et al., 2006; Tomadakis & Sotirchos, 1993). Its value is obtained knowing the pressure, the temperature, the critical pressure and critical temperature, as well as the molar mass.

As suggested by (Marangio et al., 2009), the water molar flow at the anode side, $n_{H_2O}^{an}$, can be obtained adding the net water transported through the membrane the water consumed in the oxidation reaction:

$$\dot{n}_{H_2O}^{an} = \frac{\dot{N}_{H_2O}^{mem} + \dot{N}_{H_2O}^{cons}}{A} \tag{3.31}$$

Instead, at the cathode, as stated before, there is no water consumption. Thus, the equation for computing the molar flow on the reduction electrode is:

$$\dot{n}_{H_2O}^{cat} = \frac{\dot{N}_{H_2O}^{mem}}{A} \tag{3.32}$$

- Hydraulic pressure effect $\dot{N}_{H_2O}^{pe}$

Finally, a large pressure asymmetry between the two electrodes can cause a flux of water in the membrane following the gradient. The pressure difference Δp between cathode and anode is, thus, used in the Darcy's Law to compute the molar flow. According to (Abdin et al., 2015; Awasthi et al., 2011; Kim et al., 2013; Marangio et al., 2009), the equation for computing this contribution involve the membrane permeability to water, K_{darcy}, the viscosity, μ_{H_2O}, and the molar mass of water $M_{m.H_2O}$;

$$\dot{N}_{H_2O}^{pe} = K_{darcy} \frac{A\rho_{H_2O}}{t_{mem}\mu_{H_2O}M_{m,H_2O}} \Delta p \tag{3.33}$$

K_{darcy} value can be found in literature equal to $1.58 * 10^{-18}$ m² (Medina & Santarelli, 2010).

Substituting the equations, into the equation (3.28), the resulting equation can be solved with respect to $\dot{N}_{H_2O}^{mem}$.

3.3 Energy Balance

In the equations analyzed in the previous sections, temperature is often present. Therefore, for better understanding the system a thermal balance

is added to the study, being aware of the energy required by the non-spontaneous endothermic reaction, provided in the form of electric energy.

Following the study presented by (Colbertaldo et al., 2017), the global equation can be written considering the temperature variation as a function of the enthalpy net balance, electric power contribution and heat transfer:

$$C_{tot}\frac{dT}{dt} = \dot{H}_{in} - \dot{H}_{out} - \dot{Q}_{loss} + P_{el} \qquad (3.34)$$

The term C_{tot} $\left[\frac{kJ}{K}\right]$ indicates the overall thermal capacity of the whole system taken into consideration. Through the variation of the enthalpy between the incoming and outgoing flows, $\dot{H}_{in} - \dot{H}_{out}$, the cooling contribution is taken into account being function of temperature and pressure. The term $\dot{Q}_{loss}$ is used in the equation to define the heat losses toward the ambient air through the external wall of the control volume, i.e. the stack. In the literature, the thermal power contribution is or imposed (assumed equal to zero, constant or function of the enthalpy difference) or computed by means of the heat transfer equation:

$$\dot{Q}_{loss} = UA(T_{wall} - T_{amb}) \qquad (3.35)$$

In the last case, the global heat transfer coefficient U $\left[\frac{W}{m^2 K}\right]$ must been known through manufacturer datasheet and correlations.

Lastly, P_{el} is the electric power provided by the external generator allowing the process of the electrolysis to occur. Its formulation is given in the following section.

3.4 Efficiency

In the analysis carried by (Coutanceau et al., 2018; Shiva Kumar & Himabindu, 2019; H. Zhang et al., 2010), several ways of computing the efficiencies of the electrolyzer are listed.

The following general equation is proposed by (Ni et al., 2008) and (H. Zhang et al., 2010) for the computation of the efficiency for PEMWE:

$$\eta = \frac{N_{H_2}^{out} HHV}{E + Q_{cell}\left(1 - \frac{T_0}{T_S}\right) + Q_{H_2O}\left(1 - \frac{T_0}{T_S}\right)} \qquad (3.36)$$

Here, the HHV is the higher heating value of H_2, E is the electric energy input, and Q_{H_2O} refers to the further heating provided to the water by a

second heat exchanger. By means of the temperatures of the environment T_0 and of the external heat source T_s, the distinction in the type of energy between the electric source and thermal source is considered, allowing the addition.

However, as stated in (Coutanceau et al., 2018; Shiva Kumar & Himabindu, 2019), the low operating temperature of PEM water electrolyzers allows to assume that the heat required has a low relevance with respect to the overall reaction energy. With this hypothesis, it is possible to simplify the efficiency in the equation (3.36) as only function of the cell voltage V_{EL}. The resulting formulation is, then, called voltage efficiency, $\eta_{EL,V}$.

The arithmetical steps followed to obtain the voltage efficiency from the complete equation, Eq (3.36), are explained in the following section.

- Voltage efficiency

PEM electrolyzer efficiency, in literature, can be defined as the ratio between the stored energy in the product H_2 ,as output, and the used energy in the electrolyzer, as input, (Harrison et al., 2010):

$$\eta_{EL,V} = \frac{P_{stored}}{P_{el}} \tag{3.37}$$

The used power, P_{el}, can be defined as:

$$P_{el} = IV_{EL} \tag{3.38}$$

The power stored in the H_2 , P_{stored}, corresponds to energetic value per quantity of product times the amount of product obtained. In other words, the numerator of the ratio in Eq. (3.36):

$$P_{stored} = \dot{N}_{H_2}^{out} HHV \tag{3.39}$$

The molar quantity of energy can be equally considered in the higher heating value, HHV, or in the enthalpy of the reaction $\Delta\hat{h}$. Considering the Faraday's Law applied at the Hydrogen production in Eq. (3.27), the stored power can be rewritten as:

$$P_{stored} = \dot{N}_{H_2}^{out} HHV = \frac{I}{2F} * \Delta\hat{h} \tag{3.40}$$

Therefore, combining the Eqs. (3.36) - (3.40), simplifying the current term, the resulting relationship appears as:

$$\eta_{EL,V} = \frac{\frac{\Delta\hat{h}}{2F}}{V_{EL}} \tag{3.41}$$

Finally, the term in the numerator corresponds to the thermo-neutral voltage V_{TN}, defined in (Harrison et al., 2010) as the "thermodynamic voltage required for splitting water under standard conditions" and to keep the reaction at a constant temperature. The value computed in the NREL conference paper above cited is $1.481\,V$.

- Current (Faradaic's) efficiency

However, in the real electrolyzer, because of the gas crossover in the membrane and internal parasitic currents, the amount of Hydrogen produced is not equal to theoretical amount for a defined current and voltage. The relation between the real Hydrogen flowrate and the theoretical one is called the Faradaic efficiency or current efficiency. According to (Barbir, 2005), the efficiency is defined as:

$$\eta_{EL,I} = \frac{i - i_{loss}}{i}$$

(3.42)

The actual electrolyzer efficiency is, thus, obtained in the product of the two efficiencies:

$$\eta_{EL} = \eta_{EL,V} * \eta_{EL,I}$$

(3.43)

Nevertheless, apart in case of operation at low current densities, as reported by (Barbir, 2005; Görgün, 2006; Shiva Kumar & Himabindu, 2019) the value of the current efficiency is higher than 99%.

3.5 Degradation of PEM Electrolyser

In this section, degradation phenomena are analyzed via literature review to motivate the optimization in this section. Even though, the number of studies concerning the durability of the PEM water electrolyzers is limited, especially compared to the amount of works produced for the Proton Exchange Membrane Fuel Cell (PEMFC), the results and considerations are converging in the same conclusions (Chandesris et al., 2015; Q. Feng et al., 2017; Frensch et al., 2019; Ogumerem & Pistikopoulos, 2020; Omrani & Shabani, 2021; Stucki et al., 1997).

As pointed in (Chandesris et al., 2015), PEMWE degradation, just as PEMFC, is not caused by a unique factor, but it results from the combination of thermal, chemical and mechanical stressors that appear during the operation of the water electrolyzer. Although the complexity in the processes makes difficult to perform the analysis and the experiments for

every deterioration mechanism, it has been shown that the electrolyzer performance reduction is directly interrelated to the catalysts type and catalyst layer degradation, to the membrane degradation, to the bipolar plates and current collectors corrosion. Among the listed causes, even though its thickness in the PEMWE is superior than the PEMFC, membrane pollution and reduction prevail as the main concern regarding safety, durability and performance.

Amid all the components of the PEMWE, more attention must be given to the membrane because of its important roles in gaseous products separation, protons transport, electrodes catalyst layer support. Therefore, the membrane requires an excellent chemical and thermal stability, mechanical robustness as well as resistance to gas-crossover (Q. Feng et al., 2017).

Further studies have experimentally highlighted how the degeneration of Nafion membrane, (as the most common polymer membrane used in PEMWE), is directly linked to the detectable emissions of F^- ions. Their production occurs mainly on the cathode. Here, the degrading reactions are led by the oxygen crossover from the anode to the cathode traversing the membrane, causing the membrane thinning and pollution, On the negative electrode, the oxygen reacts with the Hydrogen producing Hydrogen peroxide (H_2O_2) on the surface of the cathodic platinum catalyst. Hydrogen peroxide is, then, responsible for the generation of free radicals , such as hydroxyl and hydroperoxyl ($HO^·, HOO^·$), with the help of the metallic ions impurities inside the device that works as catalysts in the Fenton Reactions. The free radicals progressively erode the membrane on the catalyst surface without modifying the transport properties of the MEA (Chandesris et al., 2015; Frensch et al., 2019).

On one hand, it can be stated that a dissolved membrane is a possible booster of PEMWE performances, because of the connected reduction of the ohmic resistances, proportional to the membrane thickness. However, on the other hand, a thinner membrane is a smaller obstacle for gas crossover that will increase the degradation reaction as well as lead to safety issues of flammability and structural fails.

Further detailed explanation is given in the degradation model description section.

Before proceeding in the modelling of the degradation phenomena, it is interesting to briefly describe the parameters affecting the gas crossover and the degradation phenomena. From several studies, such as (Buttler & Spliethoff, 2018; Chandesris et al., 2015; N. Li et al., 2021), the physical

quantities connected with the degradation are the working temperature, the current density, the load cycling, the external load, the relative humidity and the partial pressure.

- Temperature

Among all the physical properties, the strongest impact on the PEMWE performance is given by the temperature, as stated by (Ogumerem & Pistikopoulos, 2020). From the study carried by (Diéguez et al., 2008), it is possible to understand that high operating temperature helps to improve the performance and efficiency, reducing to amount of electricity required.

However, working at high temperature has several disadvantages. Firstly, it directly causes an increase in sensitivity of the membrane to physical deformation under high pressure, especially with an operating temperature higher than 100°C (Ogumerem & Pistikopoulos, 2020). Secondly, it indirectly results in a faster membrane dissolution by increasing the kinetics of the free radicals' formation reactions and of the rates of gas crossover. In particular, it causes higher hydrogen crossover rate and hydrogen pressure on the membrane.

Also, Titanium used in bipolar plates of the water electrolyzer is affected by high heat level, that causes an acceleration of the passivation mechanism, and related long term structural problems (Frensch et al., 2019).

Moreover, inside the stack the heat generated by the joule effect is not uniform, but more intense in the area of the membrane pressed on the current contactor. As a consequence, the degradation is localized, resulting in a higher instability (H. Liu et al., 2009).

(Omrani & Shabani, 2021) have produced a more detailed study of the membrane temperature profile pointing out the presence of temperature gradient across the cell. This temperature difference is also affected and boosted by material properties, design of the flow channels, water stoichiometry, and, especially, by the current density (Stähler et al., 2020).

The attack on the membrane by the free radicals is evaluated in terms of fluoride emissions, calculated in the Fluoride Release Rate (FRR). Therefore, it is common to analyze the effect of temperature in degradation mechanism comparing it with FRR. The study carried by (H. Liu et al., 2009) reports common values of the fluoride release rate in the range $0.005-0.020 \frac{\mu g}{h*cm^2}$ for a PEM working at $50-60\,°C$, $670\,kPa$, $1.08\frac{A}{cm^2}$, in protonically transported water. The FRR analysis, performed between $55\,°C$ and $150\,°C$ by (H. Liu et al., 2009), shows an increase of about two orders of magnitude. (Frensch

et al., 2019) refers, for a PEMWE working at $2\frac{A}{cm^2}$ a increase of one order of magnitude increasing the temperature from $60\,°C$ to $90°C$.

- Current density

As mentioned in the previous sections, another parameter strongly involved in the degradation mechanism is the current density.

The effects of current density on the electrolyzer performance due to current density are studied by (Q. Feng et al., 2017). (Moshtarikhah et al., 2017; Omrani & Shabani, 2021) report, among those effects, the structural change in the membrane: an increase of the current density generates a higher membrane swelling, resulting in an increase of gas permeability. Instead, (Chandesris et al., 2015) point out that a raise in the current density corresponds to a reduction in molar percentage of oxygen at the cathode, which lead to a decrease of hydrogen peroxide and free radicals. However, also at very low current densities the degradation rate is reduced. This result comes from the balance between two competitive reactions with the same compound, the radicals $HO^·$: a reaction producing it and the reaction of its consumption in the mechanism of membrane attack. The first reaction at low current densities prevails. At working condition of $80\,°C$, atmospheric pressure and constant source of iron ions, the maximum is reached after $0.4\frac{A}{cm^2}$ and it is about equal to $2.6\frac{\mu g}{h*cm^2}$. At $60°C$, the maximum is just below $0.6\frac{\mu g}{h*cm^2}$ reached at $0.2\frac{A}{cm^2}$, as reported by the experimental results of (Chandesris et al., 2015).

Interesting experiments on the influence of the operation current on PEM water electrolyzer degradation has been performed by (Frensch et al., 2019), with a focus on the value obtained at the first hours of operation. Here, the difference in voltage variation rate is quite relevant and connected to the value of the current density. In general, it is explained that at low current densities, the voltage increase, connected to the performance worsening, is almost constant over time.

Moreover, (Lettenmeier et al., 2016), as reported by (Q. Feng et al., 2017), a high current density causes the increment of Iridium dissolution at the anode.

However, the effects of the current on the voltage variation are less relevant and more complex to define than the effects of temperature.

- Pressure

One of the advantages of the PEM electrolyzer is the possibility of operating at high pressures (> 3450 kPa),(H. Liu et al., 2009), reducing the need of a further compression in the next steps. However, working at such high operating pressure has shown relevant effects in the degradation rate of these systems.

First, before chemical degradation, mechanical stressors on the membrane are prevailing under prolonged exposure to high differential pressures in terms of the failure risk due to membrane creep and boosted crack propagation. Moreover, these operating conditions critically promote the gas cross-permeation effects (Millet, 2011). Similar to temperature effects, the pressure is directly proportional to the solubility, thus permeability, and mobility of the hydrogen and oxygen in the hydrated perfluorinated membranes (Grigoriev et al., 2009). A higher solubility in low current density operation is a source of potential significant hazards (Sakai et al., 1985). Additionally, (Q. Feng et al., 2017) report a correlation of the water starvation with high pressures, in combination with high current density, uneven water distribution and inappropriate porous current collector.

- Load cycling

(Rakousky et al., 2017) report a lower degradation rate for dynamic loading with respect to the value obtained in constant operation at high current density. However, successive studies have pointed out how results of (Rakousky et al., 2017) were mainly related to the time in which the high current is applied. The variation in the degradation rate is connected to the operation with high current density (Buttler & Spliethoff, 2018).

3.5.1   Degradation model description

In this subsection, the degradation model is explained to simulate the macroscopic effects of chemical degradation: Fluoride Release Rate FRR and membrane thinning. (Chandesris et al., 2015) base their work on the studies conducted by (Stucki et al., 1997), about detecting evidences on the phenomenon of membrane thinning, and by (Laconti et al., 2006), about localizing on the cathode the reactions of the MEA degradation, where the observed release of F^- ions is non negligible.

3.5.1.1 Gas crossover

The permeation of the gasses, H_2 and O_2, between the two electrodes is at the base of the degradation reactions. In particular, the oxygen crossing from the anode to the cathode can't be easily prevent by the Nafion®.

The physical mechanisms responsible for the membrane gas cross-over, according to (Chandesris et al., 2015), can be summarized   in two

phenomena: (1) gas concentration gradient and (2) water flow through the membrane.

- Gas concentration gradient

Both the products of the reduction and oxidation reactions, H_2 and O_2, are present, in the gas form, only at their respective electrodes, cathode and anode. Thus, the gasses, dissolved in the membrane ionomer, present a concentration difference between the two electrodes, resulting in a concentration gradient. As a consequence, two diffusive fluxes are produced: the oxygen, present in the anode side, tends towards the cathode, while the hydrogen produced at the cathode crosses the membrane to reach the anode side.

- Water flow through membrane

As described in detail in the chapter 3.2.3, electro-osmotic phenomenon, as a first cause, in combination with water diffusion and hydraulic pressure effect, generate a water flowrate through the membrane. Considering that two gases can, partially, dissolve in the water, they can also be carried by convection in the water flow. This concept is applied in the equations proposed by (Chandesris et al., 2015) to describe the transported dissolved gases as a function of the gas concentration, diffusivity in the perfluorinated membrane and of the water velocity inside the membrane.

Then, the concentration c_i of the solved species i is computed as proportional to the partial pressure P_i^j, at each current collector j considered as a frontier of the membrane:

$$c_i^j = S_i P_i^j \qquad (3.44)$$

In the proposed study, the model proceeds under the assumptions of constant partial pressure P_i^j for both species and of the same solubility of the gases in the membrane and in the water, as suggested in (Ito et al., 2011).

The literature reports several correlations of the solubility and diffusion coefficients, mostly empirically connected to the temperature and to the membrane degree of hydration. Considering a medium permeation behavior and the low impact of water uptake to fully hydrated electrolyzers, the chosen laws for the solubility and diffusivity are taken respectively from (Amphlett et al., 1995) and (Bernardi & Verbrugge, 1992) for the hydrogen and from (Parthasarathy et al., 1992) and (Wise & Houghton, 1966) for the Oxygen. The four expressions are listed in the table 3-2.

Table 3-2 O₂ and H₂ solubility and diffusivity coefficients.

Parameter [unit]	H_2	O_2
$S_i \left[\dfrac{\text{mol}}{\text{Pa} * \text{m}^3} \right]$	$\dfrac{1}{\omega * 1.09 * 10^5 * e^{\frac{77}{T}}}$ (3.45)	$1.62 * 10^{-6} * e^{\frac{603}{T}}$ (3.46)
$D_i \left[\dfrac{\text{m}^2}{\text{s}} \right]$	$1.23 * 10^{-6} * e^{-\frac{2602}{T}}$ (3.47)	$4.2 * 10^{-6} * e^{-\left(-\frac{18380}{RT}\right)}$ (3.48)

In the equations (3.45) - (3.48), the temperature T is in Kelvin and R is the universal gas constant. The equation (3.45), related to the hydrogen solubility, is the only chosen law dependent on the temperature and corrected with the water uptake, present in the term ω. This term refers to the water uptake normalized as a weight percentage of water and it is computed as:

$$\omega = \frac{\lambda M_{H_2O}}{EW} \tag{3.49}$$

Here, λ is the water uptake, M_{H_2O} is the water molar mass and EW is the weight of dry Nafion® per moles of sulfonate acid groups, namely equivalent weight. According to (Ito et al., 2011), the value of EW is equal to $1.1\ kg/mol$.

For the second mechanism behind gas crossover, the water velocity must be computed. The formulation of net flow, resulting from the three forcing phenomena, is defined in the equation (3.28). However, an empirical law is considered in the model of (Chandesris et al., 2015), interrelating the transferred water $Q_{H_2O}^t$ as a function of the consume water mass flow $Q_{H_2O}^c$ and the current density i:

$$Q_{H_2O}^t = (-0.332 \log(i) + 5.59) * Q_{H_2O}^c \tag{3.50}$$

The volumetric flow of the consumed water is obtained multiplying the molar flow, computed in (3.20), and the water molar mass over the water density:

$$Q_{H_2O}^c = \frac{M_{H_2O} * \dot{N}_{H_2O}^{cons}}{\rho_{H_2O}} \tag{3.51}$$

Finally, the water velocity is the result of the following equation:

$$v_{H_2O} = \frac{Q_{H_2O}^t}{A} \tag{3.52}$$

Where, A is the membrane surface.

At the membrane-current collector frontiers, as stated in the assumption, the partial pressures are constant. In the literature, the values are usually obtained by the molar flow balances at the electrode, from which the molar fraction of each gas times the total pressure at that electrode P^j is computed as follows:

$$P_i^j = x_i^j P^j \tag{3.53}$$

However, in this analysis, because of the lack of knowledges concerning all the side reactions and for simplicity's sake , the approach proposed in (Biaku et al., 2008) and recalled in the Eqs (3.7)- (3.8) is chosen.

3.5.1.2 Hydrogen peroxide formation

Pushed by the concentration gradient and transported by the water flow, the oxygen arrives at the cathode where it starts to take part in the oxygen reduction reactions (ORR). Considering the low potential at the cathode, lower than 0.4 V, water recombination can be neglected and the oxygen is mainly reduced through the Hydrogen peroxide formation pathway, as shown by (Ruvinskiy et al., 2011):

$$O_2 + 2H^+ + 2e^- \rightarrow H_2O_2 \tag{3.54}$$

Neglecting the reverse reaction as suggested by (Sethuraman et al., 2008), the kinetic rate of the electrochemical formation reaction is:

$$R_1 = k_1 c_{O_2} c_{H^+}^2 \tag{3.55}$$

Where c_{O_2} is the oxygen concentration, c_{H^+} is the proton concentration and k_1 is the kinetic constant per unit of electrochemical active area, which is reported by (Sethuraman et al., 2008):

$$k_1 = k_1^0 \, e^{\left(\frac{-\alpha_{H_2O_2}F}{RT^0}\eta_{2e}\right)} = k_{1_0}^0 \, e^{\left(\frac{-A_{H_2O_2}}{RT}\right)} e^{\left(\frac{-\alpha_{H_2O_2}F}{RT^0}\eta_{2e}\right)} \tag{3.56}$$

The parameters involved in the equations are reported in the following table, table 3-3, with the respective references.

Table 3-3 Parameters used in the kinetic constant rate model

Symbol	Parameter	Value [unit]	Reference
$\alpha_{H_2O_2}$	Transfer coefficient of the electrochemical reaction	0.5 [−]	(Chandesris et al., 2015)
η_{2e}	Cathodic overpotential related to the 2-electrons ORR	0.695 [V]	(Sethuraman et al., 2008)
$A_{H_2O_2}$	Activation energy of the electrochemical reaction	$42{,}450 \left[\frac{J}{mol}\right]$	(Anderson & Albu, 2000)

	on Pt/C with Nafion® electrolyte		
$k_{1_0}^0$	Kinetic constant	$7.068*10^2 \left[\dfrac{\text{m}^7}{\text{mol}^2\text{s}}\right]$	(Sethuraman et al., 2008)
T^0	Reference temperature	298 [K]	(Chandesris et al., 2015)

The thickness of the cathodic catalyst layer $e_{cl,C}$ is then considered in order to compute the formation rate normalized for the volume of the catalyst layer, corrected by the rugosity of the cathode γ_C:

$$v_1 = \frac{\gamma_C R_1}{e_{cl,C}} \tag{3.57}$$

The values of the thickness and rugosity are taken form the work of (Chandesris et al., 2015; Wong & Kjeang, 2014): $e_{cl,C}$ is assumed equal $10\ \mu m$, whereas the reported value of γ_C is 150.

For computing the value of the electrochemical formation rate in the Eq. (3.55), the concentrations of oxygen and protons must be defined. The amount of oxygen is obtained by the Eq. (3.44), considering the cathode frontier. For the hydrogen positive ions, the formulation suggested in the model, taken from (Wong & Kjeang, 2014), relates the polymer density, function of the water uptake, and the ionomer equivalent weight EW defined before:

$$c_{H^+} = \frac{\rho_M}{EW} = \frac{1980 + 32.4\lambda}{(1 + 0.0648*\lambda)EW} \tag{3.58}$$

3.5.1.3 Radical Formation

As stated before, the chemical degradation of the membrane is linked to reactions involving the free radicals, mainly hydroxyl $HO^{\cdot}$ and hydroperoxyl $HOO^{\cdot}$, and the Fenton's reactions. These compounds in the PEMWE operation result from the decomposition of Hydrogen peroxide H_2O_2. Several reactions occur in the device involving the radicals, as reactants or as products, with and without the metal ions (Fe^{2+}) as Fenton active metal. These reactions are taken from the study carried out by (Gubler et al., 2011), listed in Appendix 1. From these reactions it is possible to compute the final concentration of the $HO^{\cdot}$, intervening in the actual membrane deterioration. However, being the reactions competitive each other in production and consumption, the time evolution of the concentration of the different species ($H_2O_2, HO^{\cdot}, HOO^{\cdot}, Fe^{2+}$) has to be computed by the molar mass balance equation for each j species on the interface of the cathodic catalyst layer:

$$\frac{dc_j}{dt} = \sum_i \left(-sign(v_{ji})\delta_{ij}\right)v_i + \frac{j_j^{in}}{e_{clC}} - \frac{j_j^{out}}{e_{cl,C}} \tag{3.59}$$

Where v_i is the reaction rate of the $i - th$ chemical reaction obtained from the product of all the concentrations of the reactants j times the kinetics constant of the specific reaction i, as follows:

$$v_i = k_i \prod_j c_j \tag{3.60}$$

In the Eq. (3.59), v_{ij} is the stoichiometric coefficient, δ_{ij} is null or equal to one respectively when the j component is not or is involved in the $i - th$ reaction. The balance, then, requires the definition of the entering and exiting molar flow per unit of surface j_j at the catalyst frontier at the cathode. Apart from hydrogen peroxide with an initial contribution computed from v_1, it is assumed that a null incoming flow for all the species and an outgoing flow convectively transported by the water flow:

$$j_j^{out} = v_{H_2O} * c_j \tag{3.61}$$

3.5.1.4 Source of metallic ions
Degradation mechanism of the membrane is also dependent on the Fenton active metallic ions that contaminate the membrane. These constituents are firstly generated during corrosion of stainless steel parts and pipes in the supplying system introduced by the feed water (Chandesris et al., 2015; Q. Feng et al., 2017). Among all, as reported by (K. Feng et al., 2011; Yang et al., 2012), Fe^{2+} prevails in quantity. Its presence is shown to be proportionally linked to the final FRR parameter. In literature, the Fe^{2+} source term can be considered constant, obtained by fixing the metal ion incoming flux, current density-dependent, or computed as a function of operating temperature (Yang et al., 2012). The latter is reported as follow:

$$S_{Fe^{2+}} = S_{Fe^{2+}}^{353\,K} \frac{T - 290}{353 - 290} \tag{3.62}$$

Where $S_{Fe^{2+}}^{353\,K}$ is the constant value of Fe^{2+} source measured at $353\,K$ equal to $9 * 10^{-2} \frac{\text{mol}}{\text{m}^3\text{s}}$ (Chandesris et al., 2015).

3.5.1.5 Membrane attack mechanism and fluor formation rate
Finally, the $HO^\cdot$ produced intervenes in the decomposition of the Nafion membrane by cutting the sidechain from the backbone of the polymer, producing oxygen central radicals. Further unzipping of the radicals occurs releasing HF constituents, determining the fluoride release. The unzipping

reaction is reported by (Gubler et al., 2011), and well described in (Wong & Kjeang, 2014):

$$HO^\cdot + R_f CF_2 COOH \rightarrow products + nHF \qquad (3.63)$$
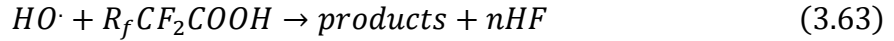
In the study carried out by (Chandesris et al., 2015), a relationship with the actually measured effective fluoride release is presented as follows:

$$v_{fluor} = 3.6 * v_{10} \qquad (3.64)$$

Where v_{10} represents the reaction rate of the chemical reaction shown in Eq (3.63), that it will be computed, according to Eq (3.60) as follows:

$$v_{10} = k_{10} * C_{HO^\cdot} * C_{membrane} \qquad (3.65)$$

where $C_{HO^\cdot}$ is the concentration of the hydroxyl free radical, $C_{membrane}$ concentration of the Nafion® membrane obtain considering the density of the Nafion® divided by the equivalent weight, above defined.

The Fluoride Release Rate (FRR), in $\frac{\mu g}{h*cm^2}$, is defined as a mass flow over the cell Area, for this reason, the volumetric concentration flow obtained in v_{fluor} is multiplied for the molar mass of the fluoride MM_{fluor} (18.998 g/mol (Information, 2021)) and for thickness of the membrane t_{mem} [cm]:

$$FRR = v_{fluor} * MM_{fluor} * t_{mem} * 3600\frac{s}{h} * 10^{-6}\frac{m^3}{cm^3} * 10^6\frac{\mu g}{g} \qquad (3.66)$$

The Fluoride ion is then related to the reduction of performance as responsible of the of the membrane thinning. For this reason the relationship with the membrane thinning rate TR, in $\frac{nm}{h}$, is also reported, according to the work of (Fouda-Onana et al., 2016) and its assumption (Nafion density 2 g/cm³ and amount of fluorine in Nafion is 82 wt.%), :

$$TR = \frac{FRR}{\rho_{Naf} * 0.82} * 10^{-6}\frac{g}{\mu g} * 10^7\frac{nm}{cm} \qquad (3.67)$$

The reduction of the membrane, in addition to a reduction of mechanical stability, generates a reduction of the ohmic resistance but a further increase in the gas crossover. This will lead to a higher risk linked to high flammability of the mixture H_2-O_2, as well as an increase of the activation overpotential. This additional contribution can be model, as suggested by (Neyerlin et al., 2005), using a Tafel-like expression:

$$V_{degr} = \frac{R * T}{F} * \ln\left[\frac{i_{H_2}}{i_{o,an}}\right] \qquad (3.68)$$

Where the current density of the Hydrogen crossover, higher than oxygen one (Chandesris et al., 2015), is computed as:

$$i_{H_2} = S_{H_2} * D_{H_2} * 2 * F * \frac{p_{H_2}}{t_{mem}} \tag{3.69}$$

After defining this system of equations, it is possible to compute the new cell voltage with the reduced membrane thickness. The model explained in this chapter is applied in the MATLAB® environment and the obtained results are explained in the next chapter.

4 Results and discussions

After examining the models present in literature for the device, the PEM electrolyzer and degradation model analysis in MATLAB® environment is presented in this chapter.

4.1 Electrochemical model results

The equations listed in the chapter 3.1 are implemented in the MATLAB® script. It is possible to further understand by visualization the influence of the different parameters on the cell voltage. In the model, apart from the parameters already set in the chapter 3, the single cell active area is assumed equal to $608 \, \text{cm}^2$ and the number of cells in a single stack equal to 102, according to (Mayyas et al., 2019).

In the figure 4-1, the polarization curve obtained is shown.
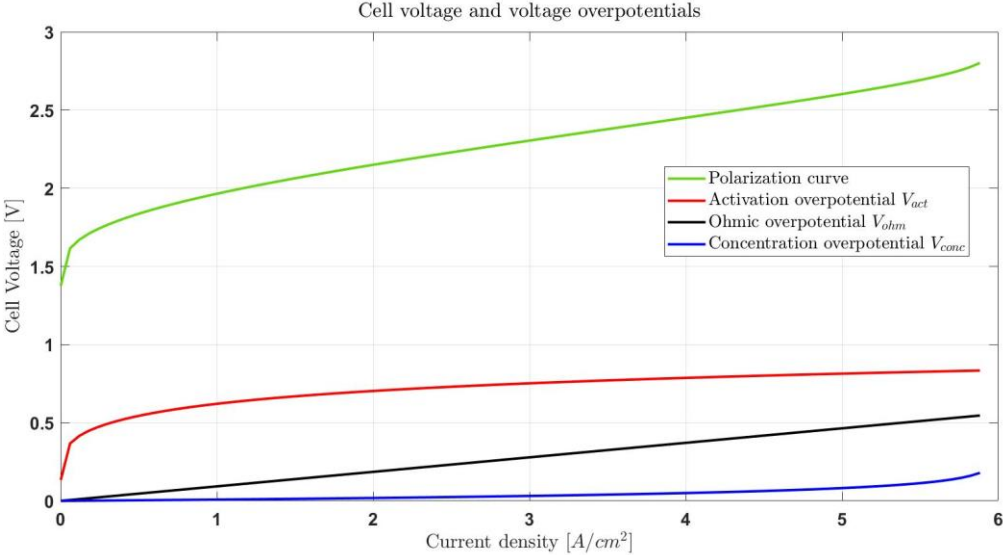
Figure 4-1 PEM electrolyzer polarization curve and voltage overpotentials

From the figure above, it is observed that the initial activation overpotential contribution increases the voltage at low current. The linear increase linked to the ohmic component of the irreversibilities in the middle part and finally

the concentration overpotential contribute towards the end of the curve. In order to display in an effective way the last overvoltage, the range of current density considered had to reach higher value than the usual operation.

From the equations provided in the section 3.2.2 and 3.4, multiplied by the number of cells of a stack, the production and power consumed are also plotted, resulting in the figure 4-2.
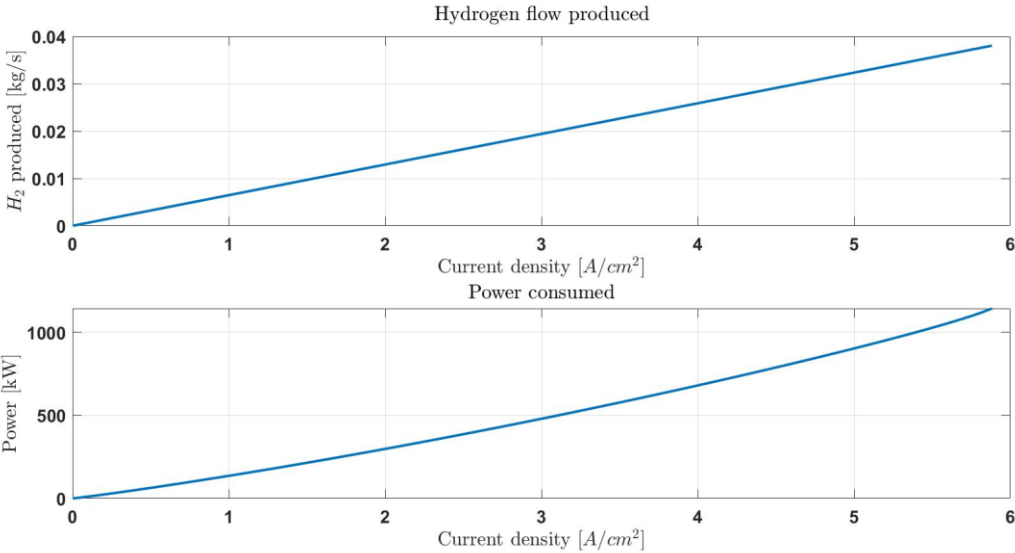
**Figure 4-2 Top: Plot of hydrogen produced vs the current density. Bottom: Power consumed vs current density.**

In both figures, it is clear how a high current density implies a high level of power consumed, despite producing more Hydrogen. The efficiency is a trade-off of the two components. However, the theoretical voltage efficiency, displayed in figure 4-3, shows a decreasing trend with respect to the current density, highlighting that the influence of the power consumption prevails. As stated in the modelling section, the current efficiency is considered equal to 1, under the hypothesis of no Faradaic losses. From the computation, the efficiency at low current densities reaches values higher than 100%. This result comes from the fact that at low current densities the cell consumes the reversible heat from the hydrolysis, with a corresponding lower power consumption than power stored (Liso et al., 2018). In real operation, the current efficiency is lower than 100%.
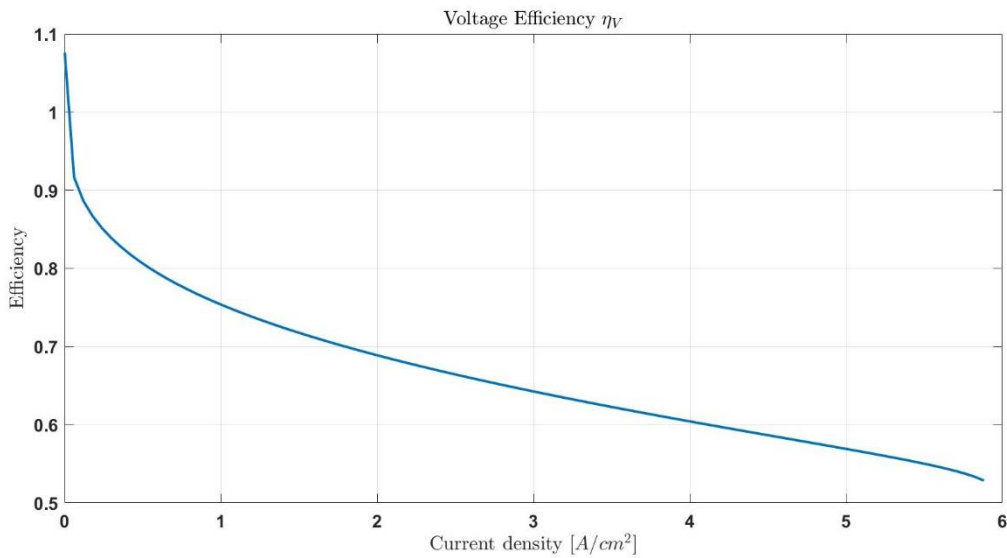
Figure 4-3 Plot of voltage efficiency vs current density

4.1.1 Sensitivity Analysis

In this section, the sensitivity analysis is performed to highlight the effect of the temperature, pressure, and current density on the voltage modelling and PEMWE degradation.
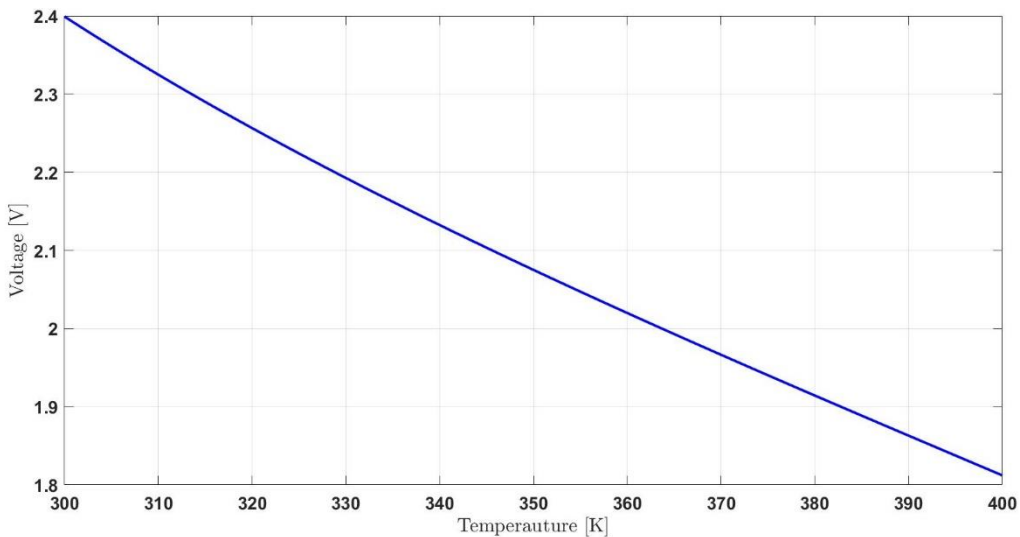
Figure 4-4 Plot of temperature dependence on theoretical electrolysis voltage at 1.47 A/cm²

From the figure 4-4, the influence of temperature appears with a reduction of voltage of -0.77 mV/K. In the electrolyzer, as pointed out in the definition of the efficiency in Eq. (3.41), a lower voltage corresponds to a better performance. Therefore, high temperatures allow higher efficiencies. The

main contribution of this reduction is linked to the decrease of the activation and ohmic overvoltage with high temperatures.

The second analysis is carried out by varying the total pressure at the electrodes.

The simulation results are shown in figure 4-5.
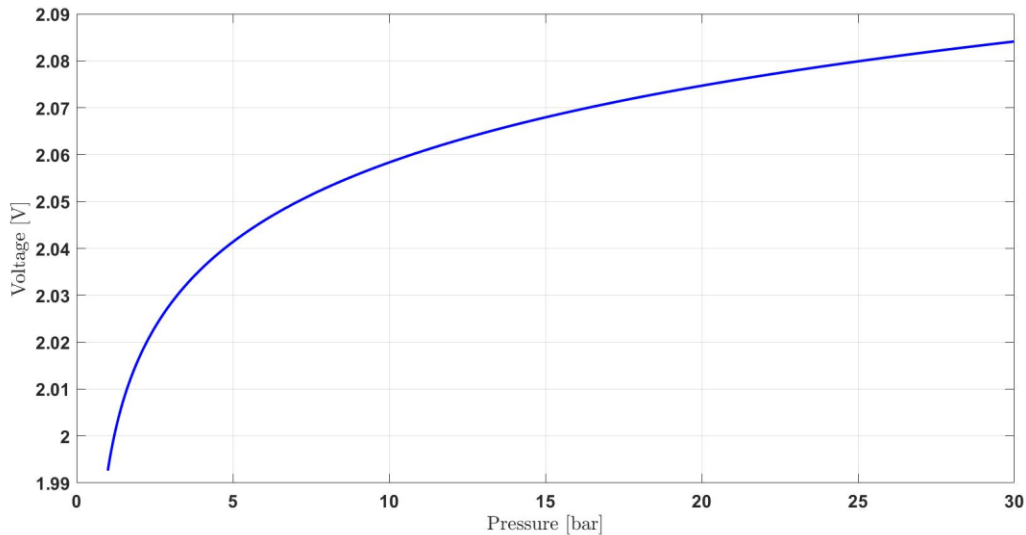
Figure 4-5 Plot of voltage vs electrode pressure.

A high pressure leads to a high voltage, reflecting in a low efficiency. The efficiency is limited to the stack performance, it does not take into account the advantages of the high-pressure operations in the total balance of plant (i.e. Elimination of one or more Hydrogen compression before storing (Hamdan, 2014)).

The results obtained are consistent with the study of (Abdin et al., 2015).

4.2 Degradation model

4.2.1   Assumptions

In this section, a list of some assumptions and simplifications that are considered for simulating the degradation is provided.

As suggested by (Chandesris et al., 2015), it is assumed that:

- the temperature is uniform inside the whole cell.
- The partial pressures at the current collector are constant.
- The solubility coefficients of the gases in water and in the membrane are almost the same.

In this work, the free radicals release phenomena are considered in absence of iron ions Fe^{2+} and Fe^{3+}. Given this simplification, the time evolution of the pollutants described in the Eq. (3.60), is studied for Hydrogen peroxide H_2O_2 and $HO^.$.Therefore, The degradation analysis considers the competitive reactions 2,6,7 of the Appendix 1. Moreover, only the steady state solutions are investigated.

4.2.2   Sensitivity Analysis

After solving the system of equations with the two concentrations as variables, their variation with respect to temperature, pressure and current density is shown in this subsection.

As displayed in the figure 4-6 and reported in the Chapter 3.5., the concentration of the Hydrogen peroxide increases with the temperature. Indeed, its production is exponentially linked to the temperature, Eq. (3.56), and prevails on its consumption, which is defined by reactions with a lower kinetics, (reactions 2 and 6 in the Appendix 1).
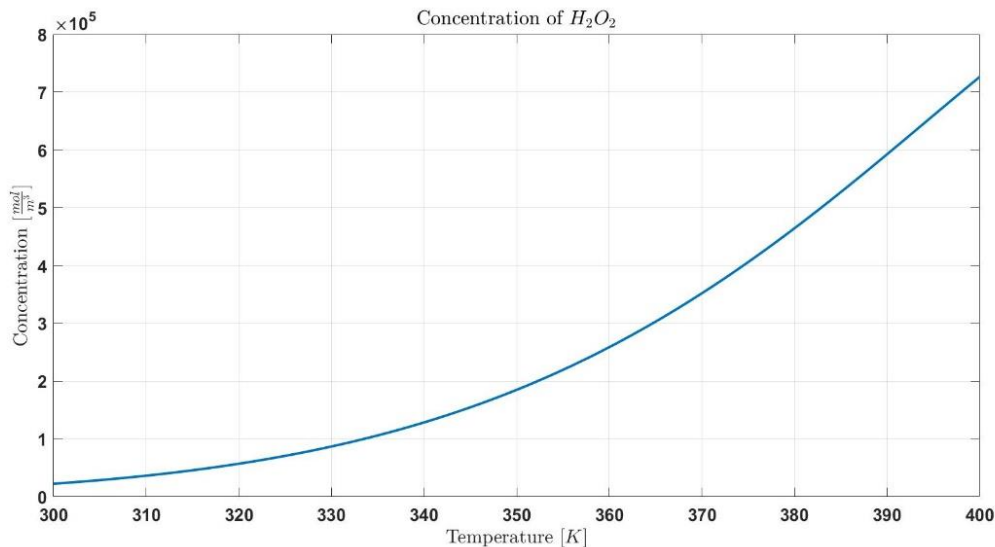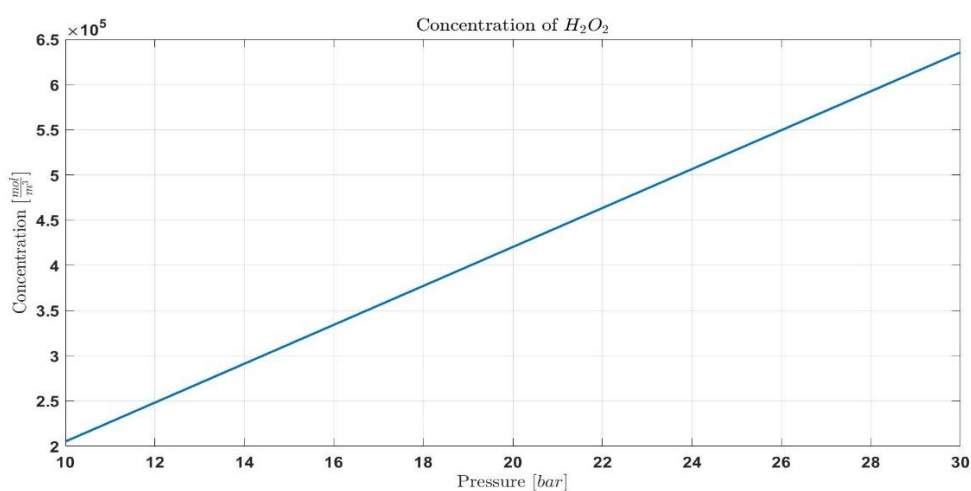

Figure 4-6 Plot of H₂O₂ concentration vs temperature at 1.47 A/cm² and 10 bar.

The influence of the pressure and current density on the concentration the hydrogen peroxide is reported in the figures 4-7 and 4-8.
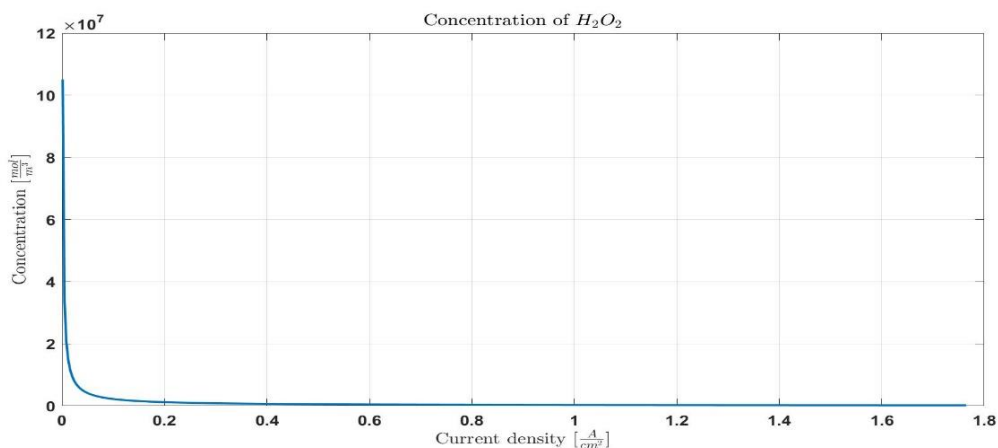
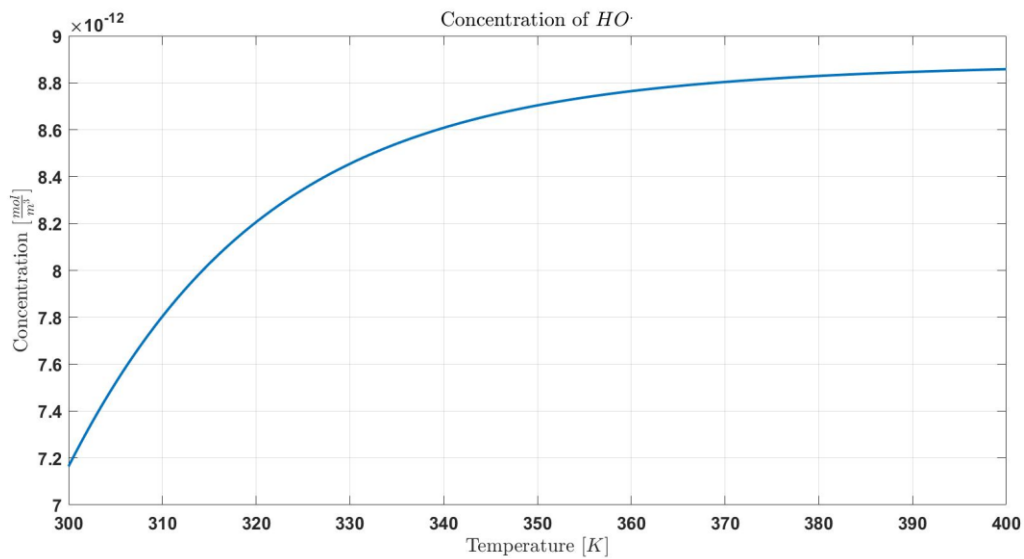**Figure 4-7 Plot of H₂O₂ concentration vs current density at 353 K and 10 bar.**

Figure 4-8 Plot of H₂O₂ concentration vs electrode pressure at 1.47 A/cm² and 353 K.

The pressure influence, displayed in the figure 4-8, derives only from the concentration of oxygen at the cathode, expressed in Eq. (3.44). While the current density variation causes the variation of the water flow.

Concerning the concentration of the hydroxyl $HO^{\cdot}$ free radical, even though it is obtained from the concentration of the H_2O_2, the concentration obtained is several orders of magnitude lower. This result is understandable considering the absence of the iron ions and the linked Fenton reactions that catalyze and boost the production of the hydroxyl free radical. In addition, it is interesting to highlight how its variation with respect to the chosen parameters is less significant than the H₂O₂ variation.

If the temperature variation generates an exponential grow in the concentration of H₂O₂, it results in a slower increase towards an asymptotic behavior for the hydroxyl, as it appears from the figure 4-9. This shows how at higher temperatures the still present influence of the temperature is

67

lower for the free radical formation. However, the thermal and mechanical stressors at higher temperatures become relevant as explained in the degradation chapter.

Figure 4-9 Plot of HO· concentration vs temperature at 1.47 A/cm² and 10 bar.
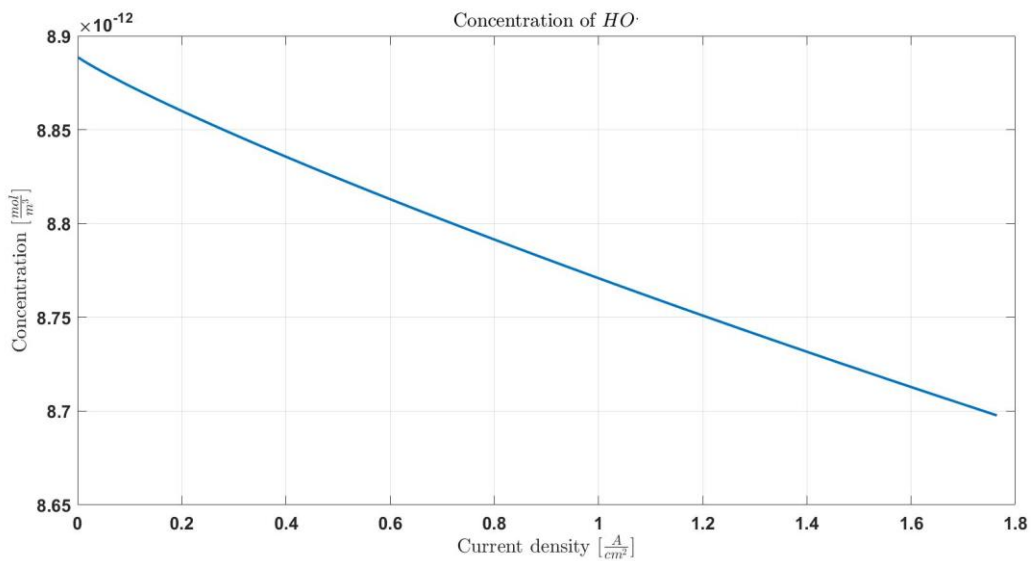
Figure 4-10 Plot of HO· concentration vs current density at 353 K and 10 atm.

In figure 4-10, a linear decrease of $HO·$ is observed as the current density increases. This behavior shows good agreement with the results obtained by (Chandesris et al., 2015). As expected, the increase at low current density described in (Chandesris et al., 2015) is absent. The reaction producing the free radical at low temperature is not present under the simplification of no iron ions. Therefore, the consumption reactions prevail over the other production reactions.
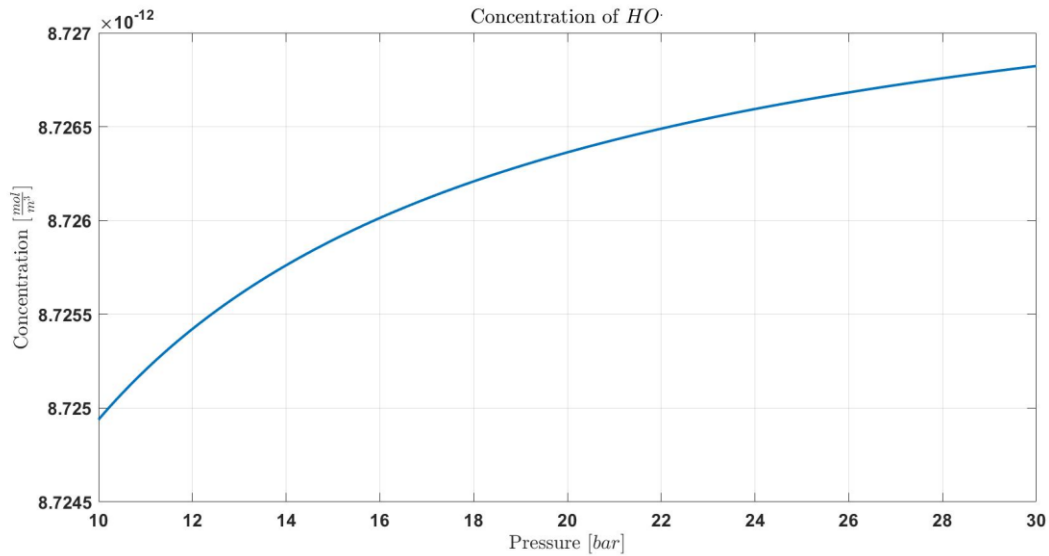
Figure 4-11 Plot of HO· concentration vs electrode pressure at 1.47 A/cm² and 353 K.

The figure 4-11 shows the increase in the concentration of HO· with increase in pressure. The critical promotion of the gas crossover and water transport at high pressures highlighted in the degradation chapter is observed here. However, the change in the hydroxyl concentration is significantly smaller when compared with the corresponding hydrogen peroxide.

As pointed out in the third chapter, the Fluoride Released Rate is associated with the dissolution of the membrane, leading to a change in the ohmic resistance and to the creation of a crossover current affecting the activation overvoltage.

Considering the degradation of the membrane after 30000 h, new overvoltages are shown in the figures 4-12 and 4-13 for different temperatures and current densities which have the main influence.
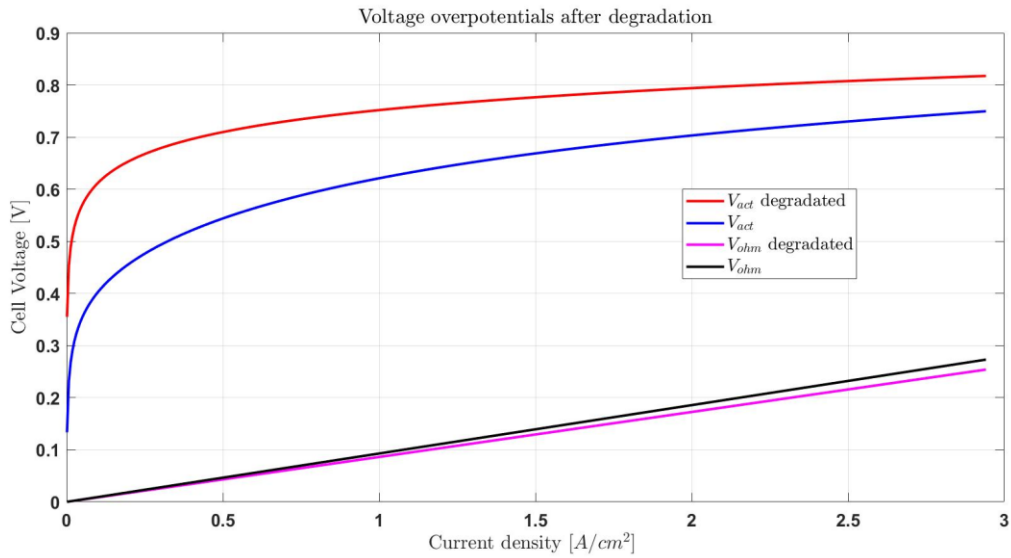
Figure 4-12 Plot of overpotentials with and without degradation at 353 K and 10 bar.

In figure 4-12, the effect of the reduction in the membrane thickness in terms of the degraded cell voltage is shown in comparison with the ideal cell voltage. The crossover current represents for the electric field an additional hurdle to overcome, dominant at low current. A thinner membrane corresponds to a lower resistance for the movement of the protons for corresponding current density. Thus, a higher activation overvoltage and a lower ohmic overvoltage are obtained.

The influence of temperature is displayed in the figure 4-13.
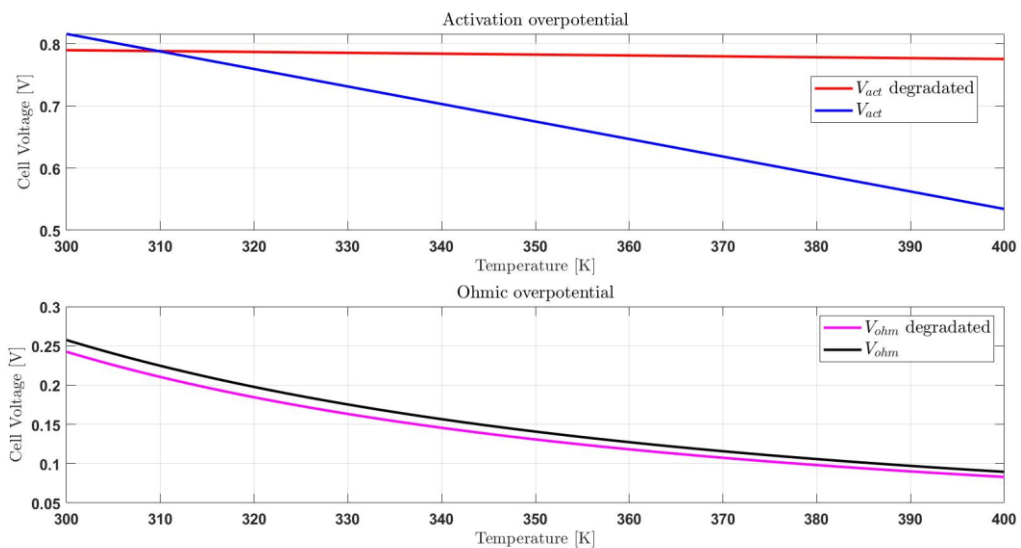
Figure 4-13 Plot of Overvoltage with and without degradation at 1.47 A/cm² and 10 bar.

For the temperature variations, it is interesting to notice that the activation overvoltage has a less steep variation with respect to temperature. This show the relevance of high temperature on the degradation.

Finally, the cell voltages are displayed.
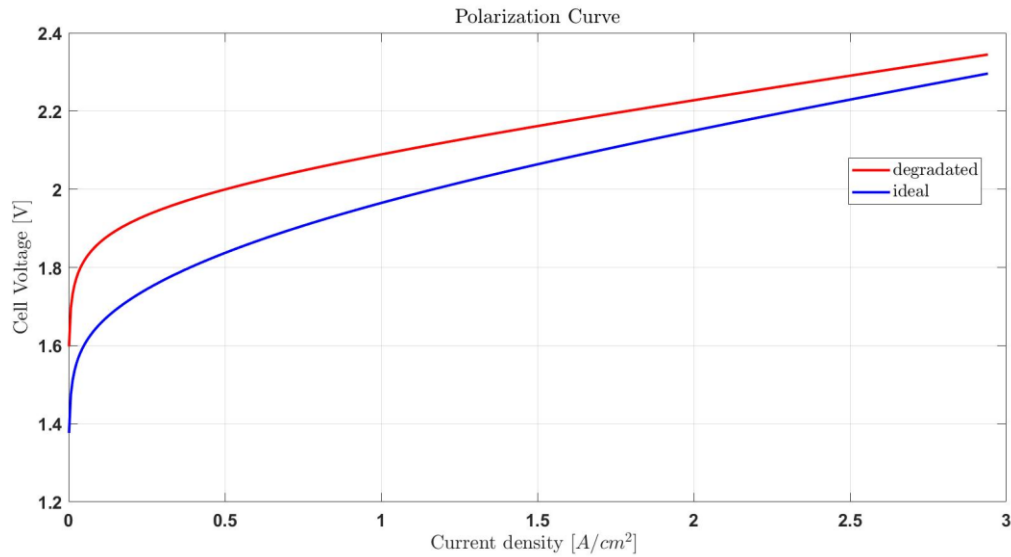
Figure 4-14 Polarization Curves

As a confirmation of the previous analysis and of (Chandesris et al., 2015), the voltage increase for degraded cell is relatively lower than the corresponding ideal cell voltage at high current densities.

5 Conclusions and Future work

5.1 Conclusions

This work aims at providing insight into the PEM water electrolyzer modelling and its degradation phenomena for optimization studies. This goal is achieved by the development of a model with and without considering the chemical degradation effect. The model is simulated under different operating conditions for sensitivity analysis associated with the cell voltage of the PEMWE performance.

In addition, the hydrogen production technologies and processes are analyzed considering the cost reduction prospective of the renewable sources, the carbon footprint and knowledge gap, for the optimal selection of the process (in this case PEMWE) to study.

From the detailed literature review of existing PEM electrolyzer models and the chemical degradation phenomenon, it is concluded that the temperature, the current density and the pressure have a relevant influence on the device performance. Even though higher efficiencies are associated with lower cell voltages and higher temperatures, such conditions cause structural weakness, thermal stressors and stronger gas crossover phenomena. The effects of current density are more complex and not clearly agreed in the literature. Among them, mechanical instability and increase in gas permeability are reported. Additionally, the pressure effect is directly linked to the mechanical stress and to the increase of water transported in the membrane.

The sensitivity analysis of the developed steady state model shows agreement with the literature. However, the results must be compared with an experimental validation that could be considered as a continuation of the thesis.

5.2 Futher work

The proposed models are developed with several assumptions and simplifications. Thus, it is open to further extension and elaborations

In the following list, some possible further works are suggested:

- As stated before, a validation experience can be set up.
- Considering the assumption of steady state, the issue of the dynamic operation is not raised, allowing a future analysis of the transient evolution of the performance and degradation.
- For further developments of the model, a simulation of the Fluoride Release Rate also considering the metal-ions source can be performed.
- As intended, the suggested future work is utilization of the developed model for optimization purpose by the total balance of plant components and the economic factors to obtain the optimal operating conditions.

References

A. Kilner, S.J. Skinner, J. C. I. and P. E. (2012). *Functional Materials for Sustainable Energy Applications*. Woodhead Publishing Series in Energy. https://www.sciencedirect.com/book/9780857090591/functional-materials-for-sustainable-energy-applications

Abdin, Z., Webb, C. J., & Gray, E. M. (2015). Modelling and simulation of a proton exchange membrane (PEM) electrolyser cell. *International Journal of Hydrogen Energy*, *40*(39), 13243–13257. https://doi.org/10.1016/j.ijhydene.2015.07.129

Amphlett, J. C., Baumert, R. M., Mann, R. F., Peppley, B. A., Roberge, P. R., & Harris, T. J. (1995). Performance Modeling of the Ballard Mark IV Solid Polymer Electrolyte Fuel Cell: I . Mechanistic Model Development. *Journal of The Electrochemical Society*, *142*(1), 1–8. https://doi.org/10.1149/1.2043866

Anderson, A. B., & Albu, T. V. (2000). Catalytic Effect of Platinum on Oxygen Reduction An Ab Initio Model Including Electrode Potential Dependence. In *Journal of The Electrochemical Society* (Vol. 147, Issue 11).

Awasthi, A., Scott, K., & Basu, S. (2011). Dynamic modeling and simulation of a proton exchange membrane electrolyzer for hydrogen production. *International Journal of Hydrogen Energy*, *36*(22), 14779–14786. https://doi.org/10.1016/j.ijhydene.2011.03.045

Ayers, K. E., Anderson, E. B., Capuano, C., Carter, B., Dalton, L., Hanlon, G., Manco, J., & Niedzwiecki, M. (2019). Research Advances towards Low Cost, High Efficiency PEM Electrolysis. *ECS Transactions*, *33*(1), 3–15. https://doi.org/10.1149/1.3484496

Badwal, S. P. S., Giddey, S., & Munnings, C. (2013). Hydrogen production via solid electrolytic routes. *Wiley Interdisciplinary Reviews: Energy and Environment*, *2*(5), 473–487. https://doi.org/10.1002/wene.50

Barbir, F. (2005). PEM electrolysis for production of hydrogen from renewable energy sources. *Solar Energy*, *78*(5), 661–669. https://doi.org/10.1016/j.solener.2004.09.003

Bernardi, D. M., & Verbrugge, M. W. (1991). Mathematical model of a gas diffusion electrode bonded to a polymer electrolyte. *AIChE Journal*, *37*(8), 1151–1163. https://doi.org/10.1002/aic.690370805

Bernardi, D. M., & Verbrugge, M. W. (1992). A Mathematical Model of the Solid-Polymer-Electrolyte Fuel Cell. *Journal of The Electrochemical Society*, *139*(9), 2477–2491. https://doi.org/10.1149/1.2221251

Bessarabov, D., & Millet, P. (2018). Brief Historical Background of Water Electrolysis. In *PEM Water Electrolysis* (pp. 17–42). Elsevier. https://doi.org/10.1016/b978-0-12-811145-1.00002-2

Bessarabov, D., Wang, H., Li, H., & Zhao, N. (2016). PEM Electrolysis for Hydrogen Production. In *PEM Electrolysis for Hydrogen Production*. CRC Press. https://doi.org/10.1201/b19096

Biaku, C. Y., Dale, N. V., Mann, M. D., Salehfar, H., Peters, A. J., & Han, T. (2008). A semiempirical study of the temperature dependence of the anode charge transfer coefficient of a 6 kW PEM electrolyzer. *International Journal of Hydrogen Energy*, *33*(16), 4247–4254. https://doi.org/10.1016/j.ijhydene.2008.06.006

BP. (2020). *BP Statistical Review of World Energy 2020*. www.bp.com/statisticalreview.

Brandon, N. P., & Kurban, Z. (2017). Clean energy and the hydrogen economy. *Phil Trans R Soc*, *375*. https://doi.org/10.1098/rsta.2016.0400

Buttler, A., & Spliethoff, H. (2018). Current status of water electrolysis for energy storage, grid balancing and sector coupling via power-to-gas and power-to-liquids: A review. *Renewable and Sustainable Energy Reviews*, *82*, 2440–2454. https://doi.org/10.1016/j.rser.2017.09.003

Carmo, M., Fritz, D. L., Mergel, J., & Stolten, D. (2013). A comprehensive review on PEM water electrolysis. In *International Journal of Hydrogen Energy* (Vol. 38, Issue 12, pp. 4901–4934). Pergamon. https://doi.org/10.1016/j.ijhydene.2013.01.151

Chandesris, M., Médeau, V., Guillet, N., Chelghoum, S., Thoby, D., & Fouda-Onana, F. (2015). Membrane degradation in PEM water electrolyzer: Numerical modeling and experimental evidence of the influence of temperature and current density. *International Journal of Hydrogen Energy*, *40*(3), 1353–1366. https://doi.org/10.1016/j.ijhydene.2014.11.111

Colbertaldo, P., Gómez Aláez, S. L., & Campanari, S. (2017). Zero-dimensional dynamic modeling of PEM electrolyzers. *Energy Procedia*, *142*, 1468–1473. https://doi.org/10.1016/j.egypro.2017.12.594

Coutanceau, C., Baranton, S., & Audichon, T. (2018). *Hydrogen Production From Water Electrolysis*. https://doi.org/10.1016/B978-0-12-811250-2.00003-0

David, M., Ocampo-Martinez, C., & Sanchez-Peña, R. (2019). Advances in Alkaline water electrolyzers: A review. *Journal of Energy Storage*, *23*, 392–403. https://doi.org/https://doi.org/10.1016/j.est.2019.03.001

Diéguez, P. M., Ursúa, A., Sanchis, P., Sopena, C., Guelbenzu, E., & Gandía, L. M. (2008). Thermal performance of a commercial alkaline water electrolyzer: Experimental study and mathematical modeling. *International Journal of Hydrogen Energy*, *33*(24), 7338–7354. https://doi.org/10.1016/j.ijhydene.2008.09.051

Dincer, I., & Acar, C. (2016). Review and Evaluation of Hydrogen Production Methods for Better Sustainability. *Alternative Energy and Ecology (ISJAEE)*, *12*(11–12), 14–36. https://doi.org/10.15518/isjaee.2016.11-12.014-036

Dutta, S., Shimpalee, S., & Van Zee, J. W. (2001). Numerical prediction of mass-exchange between cathode and anode channels in a PEM fuel cell. *International Journal of Heat and Mass Transfer*, *44*(11), 2029–2042. https://doi.org/10.1016/S0017-9310(00)00257-X

Energy: Do we have enough power to face the future? (2019). Statkraft. https://www.statkraft.com/newsroom/news-and-stories/archive/2019/energy-do-we-have-enough-power-to-face-the-future/

Environment, M. of C. and. (2021). *Norway's comprehensive climate action plan*. https://www.regjeringen.no/en/aktuelt/heilskapeleg-plan-for-a-na-klimamalet/id2827600/

Ericsson, K. (2017). *Biogenic carbon dioxide as feedstock for production of chemicals and fuels: A techno-economic assessment with a European perspective*. https://www.researchgate.net/publication/320021528_Biogenic_carbon_dioxide_as_feedstock_for_production_of_chemicals_and_fuels_A_techno-economic_assessment_with_a_European_perspective

European Commission. (2019). The European Green Deal. In *European Commission* (Vol. 53, Issue 9). https://doi.org/10.1017/CBO9781107415324.004

Feng, K., Wu, G., Li, Z., Cai, X., & Chu, P. K. (2011). *Corrosion behavior of SS316L in simulated and accelerated PEMFC environments*. https://doi.org/10.1016/j.ijhydene.2011.07.058

Feng, Q., Yuan, X. Z., Liu, G., Wei, B., Zhang, Z., Li, H., & Wang, H. (2017). A review of proton exchange membrane water electrolysis on degradation mechanisms and mitigation strategies. In *Journal of Power Sources* (Vol. 366, pp. 33–55). Elsevier B.V. https://doi.org/10.1016/j.jpowsour.2017.09.006

Fouda-Onana, F., Chandesris, M., Médeau, V., Chelghoum, S., Thoby, D., & Guillet, N. (2016). Investigation on the degradation of MEAs for PEM water electrolysers part I: Effects of testing conditions on MEA performances and membrane properties. *International Journal of Hydrogen Energy*, *41*(38), 16627–16636. https://doi.org/10.1016/j.ijhydene.2016.07.125

Frensch, S. H., Fouda-Onana, F., Serre, G., Thoby, D., Araya, S. S., & Kær, S. K. (2019). Influence of the operation mode on PEM water electrolysis degradation. *International Journal of Hydrogen Energy*, *44*(57), 29889–29898. https://doi.org/10.1016/j.ijhydene.2019.09.169

Gao, F., Blunier, B., & Miraoui, A. (2012). Proton Exchange Membrane Fuel Cells Modeling. In *Proton Exchange Membrane Fuel Cells Modeling*. John Wiley and Sons. https://doi.org/10.1002/9781118562079

García-Valverde, R., Espinosa, N., & Urbina, A. (2012). Simple PEM water electrolyser model and experimental validation. *International Journal of Hydrogen Energy*, *37*(2), 1927–1938. https://doi.org/10.1016/j.ijhydene.2011.09.027

Görgün, H. (2006). Dynamic modelling of a proton exchange membrane (PEM) electrolyzer. *Previous PDFNext PDF Article Start International Journal of Hydrogen Energy* , *31*, 29–38. https://reader.elsevier.com/reader/sd/pii/S0360319905000868?token=9F7A33DE8B 973E0CC9D6DEE88A8152593711154867BDEC58E082A50525C0828ED854FC3CDCA 5E62D226FDE9DA4C5EC3D&originRegion=eu-west- 1&originCreation=20210513151446

Grigor'ev, S. A., Khaliullin, M. M., Kuleshov, N. V., & Fateev, V. N. (2001). Electrolysis of water in a system with a solid polymer electrolyte at elevated pressure. *Russian Journal of Electrochemistry*, *37*(8), 819–822. https://doi.org/10.1023/A:1016735003101

Grigoriev, S. A., Millet, P., Korobtsev, S. V., Porembskiy, V. I., Pepic, M., Etievant, C., Puyenchet, C., & Fateev, V. N. (2009). Hydrogen safety aspects related to high-pressure polymer electrolyte membrane water electrolysis. *International Journal of Hydrogen Energy*, *34*(14), 5986–5991. https://doi.org/10.1016/j.ijhydene.2009.01.047

Gubler, L., Dockheer, S. M., & Koppenol, W. H. (2011). Radical (HO•, H• and HOO•) Formation and Ionomer Degradation in Polymer Electrolyte Fuel Cells. *Journal of The Electrochemical Society*, *158*(7), B755. https://doi.org/10.1149/1.3581040

Guo, Y., Li, G., Zhou, J., & Liu, Y. (2019). Comparison between hydrogen production by alkaline water electrolysis and hydrogen production by PEM electrolysis Comparison between hydrogen production by alkaline water electrolysis and hydrogen pro. *IOP Conference Series: Earth and Environmental Science*. https://doi.org/10.1088/1755-1315/371/4/042022

Hamdan, M. (2014). *High Pressure PEM Electrolysis Status, Key Issues, and Challenges Electrolytic Hydrogen Production Workshop NREL, Golden, Colorado*. http://www.hydrogen.energy.gov/pdfs/12021_csd_cost_

Harrison, K. W., Remick, R., Martin, G. D., & Hoskin, A. (2010). *Hydrogen Production: Fundamentals and Cas Study Summaries e Preprint*. http://www.osti.gov/bridge

Hrbek, J. (2015). *Status report on thermal gasification of biomass and waste 2019*. www.task33.ieabionenergy.com

Hydrogen Europe. (2019). *Hydrogen Europe Vision on the Role of Hydrogen and Gas Infrastructure on the Road Toward a Climate Neutral Economy-A Contribution to the Transition of the Gas Market*.

IEA. (2019). *The Future of Hydrogen* (Issue June). https://doi.org/10.1787/1e0514c4-en

IEA. (2020a). *2019 Annual Report: IEA Agreement on the production and utilizazion of hydrogen -TASK 38* (Issue September).

IEA. (2020b). *WORLD ENERGY BALANCES 2020 EDITION DATABASE DOCUMENTATION*. https://www.iea.org/subscribe-to-data-services/world-

IEAGHG. (2017a). *Technical Review Reference data and Supporting Literature Reviews for SMR Based Hydrogen Production with CCS*. www.ieaghg.org

IEAGHG. (2017b). *Techno-Economic Evaluation of SMR Based Standalone (Merchant) Plant with CCS*. www.ieaghg.org

Information, N. C. for B. (2021). *PubChem Compound Summary for CID 28179, Fluoride ion.* https://pubchem.ncbi.nlm.nih.gov/compound/28179

Ito, H., Maeda, T., Nakano, A., & Takenaka, H. (2011). Properties of Nafion membranes under PEM water electrolysis conditions. In *International Journal of Hydrogen Energy* (Vol. 36, Issue 17, pp. 10527–10540). Pergamon. https://doi.org/10.1016/j.ijhydene.2011.05.127

Kim, H., Park, M., & Lee, K. S. (2013). One-dimensional dynamic modeling of a high-pressure water electrolysis system for hydrogen production. *International Journal of Hydrogen Energy*, *38*(6), 2596–2609. https://doi.org/10.1016/j.ijhydene.2012.12.006

Kopitzke, R. W., Linkous, C. A., Anderson, H. R., & Nelson, G. L. (2000). Conductivity and Water Uptake of Aromatic-Based Proton Exchange Membrane Electrolytes. *Journal of The Electrochemical Society*, *147*(5), 1677. https://doi.org/10.1149/1.1393417

Laconti, A., Liu, H., Mittelsteadt, C., & McDonald, R. (2006). Polymer Electrolyte Membrane Degradation Mechanisms in Fuel Cells - Findings Over the Past 30 Years and Comparison with Electrolyzers. *ECS Transactions*, *1*(8), 199–219. https://doi.org/10.1149/1.2214554

Laguna-Bercero, M. A. (2012). Recent advances in high temperature electrolysis using solid oxide fuel cells: A review. In *Journal of Power Sources* (Vol. 203, pp. 4–16). Elsevier. https://doi.org/10.1016/j.jpowsour.2011.12.019

Larminie, J., & Dicks, A. (2003). *Fuel Cell Systems Explained Second Edition*. www.wiley.co.uk/fuelcellsystems.

Latrobe Valley | Hydrogen Energy Supply Chain. (n.d.). Retrieved May 4, 2021, from https://hydrogenenergysupplychain.com/latrobe-valley/

Lebbal, M. E., & Lecoeuche, S. (2009). *IDENTIFICATION AND MONITORING OF A PEM ELECTROLYSER BASED ON DYNAMICAL MODELLING*.

Lehner, M., Tichler, R., Steinmüller, H., & Koppe, M. (2014). Power-to-Gas: Technology and Business Models. In *SPRINGER BRIEFS IN ENERGY*. http://www.springer.com/series/8903

Lettenmeier, P., Wang, R., Abouatallah, R., Helmly, S., Morawietz, T., Hiesgen, R., Kolb, S., Burggraf, F., Kallo, J., Gago, A. S., & Friedrich, K. A. (2016). Durable Membrane Electrode Assemblies for Proton Exchange Membrane Electrolyzer Systems Operating at High Current Densities. *Electrochimica Acta*. https://doi.org/10.1016/j.electacta.2016.04.164

Li, N., Araya, S. S., & Kær, S. K. (2021). *Effect of Current Density , Temperature and Pressure on Proton Exchange Membrane Electrolyser Stack*. *15*(1), 15–18.

Li, X. (2005). Principles of Fuel Cells. In *Principles of Fuel Cells*. CRC Press. https://doi.org/10.1201/9780203942338

Lin, G., He, W., & Van Nguyen, T. (2004). Modeling Liquid Water Effects in the Gas Diffusion and Catalyst Layers of the Cathode of a PEM Fuel Cell. *Journal of The Electrochemical Society*, *151*(12), A1999. https://doi.org/10.1149/1.1808633

Liso, V., Savoia, G., Araya, S. S., Cinti, G., & Kær, S. K. (2018). Modelling and experimental analysis of a polymer electrolyte membrane water electrolysis cell at different operating temperatures. *Energies*, *11*(12). https://doi.org/10.3390/en11123273

Liu, H., Coms, F. D., Zhang, J., Gasteiger, H. A., & LaConti, A. B. (2009). Chemical Degradation: Correlations Between Electrolyzer and Fuel Cell Findings Han. In F. N. Büchi, M. Inaba, & T. J. Schmidt (Eds.), *Polymer Electrolyte Fuel Cell Durability* (pp. 71–115). Springer. https://doi.org/10.1016/B978-0-12-811459-9.00005-0

Liu, Ke, Cui, Z., & Fletcher, T. H. (2009). Coal Gasification. In *Hydrogen and Syngas Production and Purification Technologies* (pp. 156–218). John Wiley & Sons, Inc. https://doi.org/10.1002/9780470561256.ch4

Liu, Ke, Deluga, G. D., Bitsch-Larsen, A., Schmidt, L., & Zhang, L. (2009). Catalytic Partial Oxidation and Autothermal Reforming. In K Liu, C. Song, & V. Subramani (Eds.), *Hydrogen and Syngas Production and Purification Technologies* (pp. 127–155). https://www.wiley.com/en-us/Hydrogen+and+Syngas+Production+and+Purification+Technologies-p-9780470561249

Marangio, F., Santarelli, M., & Calì, M. (2009). Theoretical model and experimental analysis of a high pressure PEM water electrolyser for hydrogen production. *International Journal of Hydrogen Energy*, *34*(3), 1143–1158. https://doi.org/10.1016/j.ijhydene.2008.11.083

Mayyas, A., Ruth, M., Pivovar, B., Bender, G., Wipke, K., Mayyas, A., Ruth, M., Pivovar, B., Bender, G., & Wipke, K. (2019). Manufacturing Cost Analysis for Proton Exchange Membrane Water Electrolyzers. *National Renewable Energy Laboratory*, *August*, 65. https://www.nrel.gov/docs/fy10osti/72740.pdf.%0Ahttps://www.nrel.gov/docs/fy10osti/72740.pdf

Medina, P., & Santarelli, M. (2010). Analysis of water transport in a high pressure PEM electrolyzer. *International Journal of Hydrogen Energy*, *35*(11), 5173–5186. https://doi.org/10.1016/j.ijhydene.2010.02.130

Mendes, D., Mendes, A., Madeira, L. M., Iulianelli, A., Sousa, J. M., & Basile, A. (2010). The water-gas shift reaction: From conventional catalytic systems to Pd-based membrane reactors- A review. *Asia-Pacific Journal of Chemical Engineering*, *5*(1), 111–137. https://doi.org/10.1002/apj.364

Millet, P. (2011). Membrane electrolysers for hydrogen (H2) production. In *Advanced Membrane Science and Technology for Sustainable Energy and Environmental Applications* (pp. 568–609). Elsevier Inc.

https://doi.org/10.1533/9780857093790.4.568

Mitchell, R. H., & Keays, R. R. (1981). Abundance and distribution of gold, palladium and iridium in some spinel and garnet lherzolites: implications for the nature and origin of precious metal-rich intergranular components in the upper mantle. *Geochimica et Cosmochimica Acta*, *45*(12), 2425–2442. https://doi.org/10.1016/0016-7037(81)90096-X

Moshtarikhah, S., W Oppers, N. A., de Groot, M. T., F Keurentjes, J. T., Schouten, J. C., van der Schaaf, J., & van der Schaaf jvanderschaaf, J. (2017). Nernst-Planck modeling of multicomponent ion transport in a Nafion membrane at high current density. *J Appl Electrochem*, *47*, 51–62. https://doi.org/10.1007/s10800-016-1017-2

Neyerlin, K. C., Gasteiger, H. A., Mittelsteadt, C. K., Jorne, J., & Gu, W. (2005). Effect of Relative Humidity on Oxygen Reduction Kinetics in a PEMFC. *Journal of The Electrochemical Society*, *152*(6), A1073. https://doi.org/10.1149/1.1897368

Ni, M., Leung, M. K. H., & Leung, D. Y. C. (2008). Energy and exergy analysis of hydrogen production by a proton exchange membrane (PEM) electrolyzer plant. *Energy Conversion and Management*, *49*(10), 2748–2756. https://doi.org/10.1016/j.enconman.2008.03.018

Nikolaidis, P., & Poullikkas, A. (2017). A comparative overview of hydrogen production processes. In *Renewable and Sustainable Energy Reviews* (Vol. 67, pp. 597–611). Elsevier Ltd. https://doi.org/10.1016/j.rser.2016.09.044

Ogumerem, G. S., & Pistikopoulos, E. N. (2020). Parametric optimization and control for a smart Proton Exchange Membrane Water Electrolysis (PEMWE) system. *Journal of Process Control*, *91*, 37–49. https://doi.org/10.1016/j.jprocont.2020.05.002

Omrani, R., & Shabani, B. (2021). Hydrogen crossover in proton exchange membrane electrolysers: The effect of current density, pressure, temperature, and compression. *Electrochimica Acta*, *377*, 138085. https://doi.org/10.1016/j.electacta.2021.138085

Onda, K., Murakami, T., Hikosaka, T., Kobayashi, M., Notu, R., & Ito, K. (2002). Performance Analysis of Polymer-Electrolyte Water Electrolysis Cell at a Small-Unit Test Cell and Performance Prediction of Large Stacked Cell. *Journal of The Electrochemical Society*, *149*(8), A1069. https://doi.org/10.1149/1.1492287

Parry, S. J. (1984). Abundance and distribution of palladium, platinum, iridium and gold in some oxide minerals. *Chemical Geology*, *43*(1–2), 115–125. https://doi.org/10.1016/0009-2541(84)90142-6

Parthasarathy, A., Srinivasan, S., Appleby, A. J., & Martin, C. R. (1992). Temperature Dependence of the Electrode Kinetics of Oxygen Reduction at the Platinum/Nafion® Interface—A Microelectrode Investigation. *Journal of The Electrochemical Society*, *139*(9), 2530–2537. https://doi.org/10.1149/1.2221258

Proost, J. (2018). *State-of-the art CAPEX data for water electrolysers, and their impact on renewable hydrogen price settings*.

Proost, J. (2020). Critical assessment of the production scale required for fossil parity of green electrolytic hydrogen. *International Journal of Hydrogen Energy*, *45*(35), 17067–17075. https://doi.org/10.1016/j.ijhydene.2020.04.259

Rakousky, C., Reimer, U., Wippermann, K., Kuhri, S., Carmo, M., Lueke, W., & Stolten, D. (2017). Polymer electrolyte membrane water electrolysis: Restraining degradation in the presence of fluctuating power. *Journal of Power Sources*, *342*, 38–47. https://doi.org/10.1016/j.jpowsour.2016.11.118

Ritter, J. A., & Ebner, A. D. (2007). State-of-the-art adsorption and membrane separation processes for hydrogen production in the chemical and petrochemical industries. In *Separation Science and Technology* (Vol. 42, Issue 6, pp. 1123–1193). https://doi.org/10.1080/01496390701242194

Ruvinskiy, P. S., Bonnefont, A., Pham-Huu, C., & Savinova, E. R. (2011). Using ordered carbon nanomaterials for shedding light on the mechanism of the cathodic oxygen reduction reaction. *Langmuir*, *27*(14), 9018–9027. https://doi.org/10.1021/la2006343

Sakai, T., Takenaka, H., Wakabayashi, N., Kawami, Y., & Torikai, E. (1985). Gas Permeation Properties of Solid Polymer Electrolyte (SPE) Membranes. *Journal of The Electrochemical Society*, *132*(6), 1328–1332. https://doi.org/10.1149/1.2114111

Santarelli, M. G., Torchio, M. F., & Cochis, P. (2006). Parameters estimation of a PEM fuel cell polarization curve and analysis of their behavior with temperature. *Journal of Power Sources*, *159*(2), 824–835. https://doi.org/10.1016/j.jpowsour.2005.11.099

SBC Energy Institute. (2014). *Leading the Energy Transition Factbook, Hydrogen-based energy conversion - More than storage: system flexibility*. *February*, 280. http://www.sbc.slb.com/sbcinstitute.aspx,

Schmidt, O., Gambhir, A., Staffell, I., Hawkes, A., Nelson, J., & Few, S. (2017). Future cost and performance of water electrolysis: An expert elicitation study. *International Journal of Hydrogen Energy*, *42*, 30470–30492. https://doi.org/10.1016/j.ijhydene.2017.10.045

Selman, J. R., & Tobias, C. W. (1978). Mass-transfer measurements by the limiting-current technique. *Advances in Chemical Engineering*, *10*(C), 211–318. https://doi.org/10.1016/S0065-2377(08)60134-9

Sethuraman, V. A., Weidner, J. W., Haug, A. T., Motupally, S., & Protsailo, L. V. (2008). Hydrogen Peroxide Formation Rates in a PEMFC Anode and Cathode. *Journal of The Electrochemical Society*, *155*(1), B50. https://doi.org/10.1149/1.2801980

Shiva Kumar, S., & Himabindu, V. (2019). Hydrogen production by PEM water electrolysis – A review. *Materials Science for Energy Technologies*, *2*(3), 442–454. https://doi.org/10.1016/j.mset.2019.03.002

Skar, C., Jaehnert, S., Tomasgard, A., Midthun, K., & Fodstad, M. (2018). *Norway's role as a flexibility provider in a renewable Europe*.

Slade, S., Campbell, S. A., Ralph, T. R., & Walsh, F. C. (2002). Ionic Conductivity of an Extruded Nafion 1100 EW Series of Membranes. *Journal of The Electrochemical Society*, *149*(12), A1556. https://doi.org/10.1149/1.1517281

Springer, T. E., Zawodzinski, T. A., & Gottesfeld, S. (1991). Polymer Electrolyte Fuel Cell Model. *Journal of The Electrochemical Society*, *138*(8), 2334–2342. https://doi.org/10.1149/1.2085971

Stähler, M., Stähler, A., Scheepers, F., Carmo, M., Lehnert, W., & Stolten, D. (2020). Impact of porous transport layer compression on hydrogen permeation in PEM water electrolysis. *International Journal of Hydrogen Energy*, *45*(7), 4008–4014. https://doi.org/10.1016/j.ijhydene.2019.12.016

Stucki, S., Scherer, G. G., Schlagowski, S., & Fischer, E. (1997). *PEM water electrolysers: evidence for membrane failure in 100 kW demonstration plants*.

Subramani, V., Sharma, P., Zhang, L., & Liu, K. (2010). Catalytic Steam Reforming Technology for the Production of Hydrogen and Syngas. In Ke Liu, C. Song, & V. Subramani (Eds.), *Hydrogen and Syngas Production and Purification Technologies* (pp. 14–126). https://www.wiley.com/en-

us/Hydrogen+and+Syngas+Production+and+Purification+Technologies-p-9780471719755

Tomadakis, M. M., & Sotirchos, S. V. (1993). Ordinary and transition regime diffusion in random fiber structures. *AIChE Journal*, *39*(3), 397–412. https://doi.org/10.1002/aic.690390304

Ursúa, A., Gandía, L. M., & Sanchis, P. (2012). Hydrogen production from water electrolysis: Current status and future trends. *Proceedings of the IEEE*, *100*(2), 410–426. https://doi.org/10.1109/JPROC.2011.2156750

Voldsund, M., Jordal, K., & Anantharaman, R. (2016). Hydrogen production with CO2 capture. In *International Journal of Hydrogen Energy* (Vol. 41, Issue 9, pp. 4969–4992). Elsevier Ltd. https://doi.org/10.1016/j.ijhydene.2016.01.009

Wang, R., & Rohr, D. (2002). Natural gas processing technologies for large scale solid oxide fuel cells. *ACS Division of Fuel Chemistry, Preprints*, *47*(2), 506–507.

Wise, D. L., & Houghton, G. (1966). The diffusion coefficients of ten slightly soluble gases in water at 10-60°C. *Chemical Engineering Science*, *21*(11), 999–1010. https://doi.org/10.1016/0009-2509(66)85096-0

Wong, K. H., & Kjeang, E. (2014). Macroscopic In-Situ Modeling of Chemical Membrane Degradation in Polymer Electrolyte Fuel Cells. *Journal of The Electrochemical Society*. https://doi.org/10.1149/2.0031409jes

Xu, H., Chen, B., & Ni, M. (2016). Modeling of Direct Carbon-Assisted Solid Oxide Electrolysis Cell (SOEC) for Syngas Production at Two Different Electrodes. *Journal of The Electrochemical Society*, *163*(11), F3029–F3035. https://doi.org/10.1149/2.0041611jes

Yang, Y., Guo, L., & Liu, H. (2012). Factors affecting corrosion behavior of SS316L as bipolar plate material in PEMFC cathode environments. *International Journal of Hydrogen Energy*, *37*(18), 13822–13828. https://doi.org/10.1016/j.ijhydene.2012.04.026

Zeng, K., & Zhang, D. (2010). Recent progress in alkaline water electrolysis for hydrogen production and applications. In *Progress in Energy and Combustion Science* (Vol. 36, Issue 3, pp. 307–326). Pergamon. https://doi.org/10.1016/j.pecs.2009.11.002

Zhang, F., Zhao, P., Niu, M., & Maddy, J. (2016). The survey of key technologies in hydrogen energy storage. In *International Journal of Hydrogen Energy* (Vol. 41, Issue 33, pp. 14535–14552). Elsevier Ltd. https://doi.org/10.1016/j.ijhydene.2016.05.293

Zhang, H., Lin, G., & Chen, J. (2010). Evaluation and calculation on the efficiency of a water electrolysis system for hydrogen production. *International Journal of Hydrogen Energy*, *35*(20), 10851–10858. https://doi.org/10.1016/j.ijhydene.2010.07.088

Zhang, X., Chan, S. H., Ho, H. K., Tan, S. C., Li, M., Li, G., Li, J., & Feng, Z. (2015). Towards a smart energy network: The roles of fuel/electrolysis cells and technological perspectives. In *International Journal of Hydrogen Energy* (Vol. 40, Issue 21, pp. 6866–6919). Elsevier Ltd. https://doi.org/10.1016/j.ijhydene.2015.03.133

Appendices

Appendix 1: Overview of the Free Radicals Reactions

Appendix 2: Geometrical and Physical Parameters

Appendix 3: MATLAB® Code for Steady State and Degradation

Appendix 1: Overview of the Free Radicals Reactions

From the work of (Gubler et al., 2011), (Sethuraman et al., 2008) and (Wong & Kjeang, 2014) the following are the chemical reactions involving the radicals in the PEMWE operation.

#	Reaction	Kinetic constant
2	$H_2O_2 \rightarrow 2HO\cdot$	$k_2 = 1.2 * 10^{-7} \ [s^{-1}]$
3	$H_2O_2 + Fe^{2+} \rightarrow Fe^{3+} + HO\cdot + HO^-$	$k_3 = 1.05 * 10^5 e^{-\frac{9460}{RT}} \left[\frac{m^3}{mol * s}\right]$
4	$H_2O_2 + Fe^{3+} \rightarrow Fe^{2+} + HOO\cdot + H^+$	$k_4 = 4 * 10^{-8} \left[\frac{m^3}{mol * s}\right]$
5	$HO\cdot + Fe^{2+} \rightarrow Fe^{3+} + HO^-$	$k_5 = 2.3 * 10^5 \left[\frac{m^3}{mol * s}\right]$
6	$H_2O_2 + HO\cdot \rightarrow HOO\cdot + H_2O$	$k_6 = 2.7 * 10^4 \left[\frac{m^3}{mol * s}\right]$
7	$O_2 + HO\cdot \rightarrow +HOO\cdot + H_2O$	$k_7 = 1.2 * 10^7 \left[\frac{m^3}{mol * s}\right]$
8	$HOO\cdot + Fe^{3+} \rightarrow Fe^{2+} + O_2 + H^+$	$k_8 = 2 * 10^1 \left[\frac{m^3}{mol * s}\right]$
9	$HOO\cdot + Fe^{2+} + H^+ \rightarrow Fe^{3+} + H_2O_2$	$k_9 = 1.2 * 10^3 \left[\frac{m^3}{mol * s}\right]$
10	$HO\cdot + R_f - CF_2COOH \rightarrow products + HF$	$k_{10} \cong 10^3 \left[\frac{m^3}{mol * s}\right]$

Appendix 2: Geometrical and Physical Parameters

Parameter	Symbol	Value [unit]	Reference
Faraday's constant	F	$96485 \left[\frac{A\,s}{mol}\right]$	-
Gas constant	R	$8.314 \left[\frac{J}{K*mol}\right]$	-
Single cell active area	A	$608 \,[cm^2]$	(Mayyas et al., 2019)
Number of cells per stack	N_{cell}	102	(Mayyas et al., 2019)
Charge transfer coefficient	α	0.5	(Colbertaldo et al., 2017)
Limiting current density	i_L	$6 \left[\frac{A}{cm^2}\right]$	(García-Valverde et al., 2012)
Initial membrane thickness	$t_{mem,0}$	$178 \,[\mu m]$	(Chandesris et al., 2015)
Membrane hydration	λ	20	(Awasthi et al., 2011)
Water molar weight	MM_{H_2O}	$18 \left[\frac{g}{mol}\right]$	-
Water density	ρ_{H_2O}	$997 \left[\frac{kg}{m^3}\right]$	-
Thermoneutral voltage	V_{TN}	$1.481 \,[V]$	(Harrison et al., 2010)
Nafion dry membrane density	ρ_{Naf}	$1980 \left[\frac{kg}{m^3}\right]$	(Wong & Kjeang, 2014)
Nafion equivalent weight	EW	$1.1 \left[\frac{kg}{mol}\right]$	(Sethuraman et al., 2008)
Rugosity	γ_C	$150 \left[\frac{m^2}{m^2}\right]$	(Chandesris et al., 2015)
Thickness of the cathodic catalyst layer	$e_{cl,C}$	$10 \,[\mu m]$	(Wong & Kjeang, 2014)
Molar mass of the fluoride ions	MM_{fluor}	$18.998 \left[\frac{g}{mol}\right]$	(Information, 2021)

Appendix 3: MATLAB® Code for Steady State and Degradation

The script for the simulation of the model in MATLAB® environment is presented here.

Properties Definition

```matlab
classdef ELCellStack
properties
% Input parameters
R = 8.314; % Ideal gas constant [J/mol/K]
F = 96485; % Faraday's constant [C]
A = 680 % Area of cell [cm^2]
N_cells = 102; % Number of cells
Alpha = 0.5; % Transfer coefficient
il= 6; % Limiting current density [A/cm^2]
lm = 1.78*10^-2; % Membrane thickness [cm]
lambdam = 20; % Membrane hydration parameter
roughness_an=7.23*10^2; % roughness factor [cm^2/cm^2]
roughness_cat= 2.33*10^2; %roughness factor[cm^2/cm^2]
i0ref_an=2.3*10^(-7); % anode exchange current density at the reference temperature [A/cm^2]
i0ref_cat=1*10^(-3); % cathode exchange current density at the reference temperature [A/cm^2]
vthn=1.481; %thermobeutral voltage [V]
MmH2O=18; % water  molar mass [g/mol]
rhoH2O=997; % water density [kg/m^3]
Ea_an=76000; % anode activation energy [J/mol]
Ea_cat=4300; % cathode activation energy [J/mol]
Tref=298; % reference temperature [K]
end
end
```

Open Circuit Voltage

```matlab
function ENernst=ENernst(Tk,pres)
a=ELCellStack;
pcat=pres; %pressure at the cathode [bar]
pan=pres;  %pressure at the anode [bar]
ppH2=pan-PsatH2O(Tk); %partial pressure Hydrogen [bar]
ppO2=pcat-PsatH2O(Tk);%partial pressure Oxygen [bar]
E=1.229-0.9*10^(-3)*(Tk-298); %standard potential [V]
Gf_liq=E*2*a.F; % Gibbs free energy [J/mol]
ENernst=Gf_liq./(2.*a.F) - ((a.R.*Tk).*log(PsatH2O(Tk)./(ppH2.*(ppO2.^0.5)))).(2.*a.F); %[V]
end
```

Activation Overvoltage

```matlab
function Vact=VAct(Tk,I)
a=ELCellStack;
%exchange current density
i0_an=a.roughness_an*a.i0ref_an*exp(-(a.Ea_an/a.R).*(1./Tk-1/353)); % [A/cm^2]
i0_cat=a.roughness_cat*a.i0ref_cat*exp(-(a.Ea_cat/a.R).*(1./Tk-1/353));% [A/cm^2]
c =a.R.*Tk./(a.Alpha.*a.F);
b1=asinh((I./a.A)./(2.*i0_an));
```

```
b2=asinh((I./a.A)./(2.*i0_cat));
Vact=c.*(b1+b2); % [V]
end
```

Ohmic Overvoltage

```
function VOhm=VOhm(Tk,I)
a=ELCellStack;
%Area Specific ohmic Resistance
r=a.lm * 1 ./ (( 0.005139 *a.lambdam + 0.00326 )* exp(1267*(1/303-1./Tk))); %[Ohm*cm^2]
VOhm = ((I/a.A).*r); %[V]
end
```

Concentration Overvoltage

```
function VConc=VConc(Tk,I)
a=ELCellStack;
VConc = a.R.*Tk./(2*a.F).*(1+1/a.Alpha).*log(a.il./(a.il-(I./a.A))); %[V]
end
```

Water Saturation Pressure

```
function PsatH2O=PsatH2O(Tk)
Tc=Tk-273.15;
PsatH2O=610*10^(-5)*exp((Tc./(Tc+238.3))*17.2694); %[bar]
end
```

Pollutant Concentration

```
function [CH2O2,CHO]=conc(Tk,I,pres)
i=I./(a.A*10^(-4));
eta=0.695; %Equilibrium overpotential 2e-ORR  [V]
pO2=pres-PsatH2O(Tk); % Oxygen partial pressure [bar]
sO2=1.62*10^(-6)*exp(603./Tk)*10^5; % Oxygen solubility [mol/m^3/bar]
cO2=sO2.*pO2; %Oxygen concentration [mol/m^3]
Qc=a.MmH2O*i*(a.A*10^(-4))./(2*a.F*a.rhoH2O*10^3); % consumed waterflow [m^3/s]
Qt=(-0.332.*log(i)+5.59).*Qc; % transferred waterflow [m^3/s]
vH2O=Qt./(a.A*10^(-4)); % water velocity [m/s]
EW=1.100; % Nafion equivalent weight [kg/mol]
rhonaf=1980; % Nafion dry membrane density [kg/m^3]
Cmemb=rhonaf/EW; % Membrane concentration [mol/m^3]
eclc=1*10^(-5); %thickness cathode catalyst layer [m]
gammac=150; % rugosity cathode [m^2/m^2]
k1o=7.068*10^2; % Kinetic constant [m^7/mol^2/s]
AH2O2=42450; % Activation energy [J/mol]
alfa=0.5; %Trasfers coefficient of the reaction [-]
cH=(1980+32.4*a.lambdam)./((1+0.0648*a.lambdam)*(EW));
k1=k1o*exp(-AH2O2./(a.R.*Tk))*exp(-alfa*a.F*eta./(a.R.*a.Tref)); % Kinetic constant
[m^7/mol^2/s]
R1=k1.*cO2.*cH^2; % Kinetic rate [mol/m^2/s]
v1=gammac*R1./eclc; % Formation rate [mol/m^3/s]
k2=1.2*10^(-7);% Kinetic constant [s^(-1)]
```

```
k6=2.7*10^(4);% Kinetic constant [m^3/mol/s]
k7=1.2*10^(7); % Kinetic constant [m^3/mol/s]
k10=10^(3); % Kinetic constant [m^3/mol/s]
e=k7.*cO2+k10.*Cmemb-vH2O./eclc;
A2=-3*k2+vH2O./eclc;
B=e.*vH2O./(eclc*k6)-v1-e.*k2/k6;
C=-e.*v1./k6;
CH2O2=(-B+sqrt(B.^2-4.*A2.*C))./(2.*A2); % Hydrogen peroxide concetration [mol/m^3]
CHO=vH2O./(eclc*k6)-k2/k6-v1./(k6.*CH2O2); % Hydroxil concentration [mol/m^3]
end
```

Fluoride Release Rate FRR and Reduced Membrane

```
function [FRR lm]=FRRlm(CHO,t)
k10=10^(3);% Kinetic constant [m^3/mol/s]
EW=1.100; % Nafion equivalent weight [kg/mol]
rhonaf=1980; % Nafion dry membrane density [kg/m^3]
Cmemb=rhonaf/EW;   % Membrane concentration [mol/m^3]
v10=k10.*CHO.*Cmemb; % Chemical reaction rate [mol/m^3/s]
vF=3.6*v10; % F- Formation rate [mol/m^3/s]
MMF=18.998403; %Molar mass of the fluoride ions [g/mol]
FRR=vF.*MMF.*(a.lm*10^(-2)).*3600/(10^4); % Fluoride Release Rate [g/cm^2/h]
TR=FRR./(0.82*2); %thickness reduction rate [cm/h]
if TR>0
lm=a.lm-TR.*t; % membrane thickness [cm]
else
    lm=a.lm;
end
end
```

Activation Overvoltage with the Variable Membrane Thickness

```
function Vact_deg=VAct_deg(Tk,I,pres,lm)
a=ELCellStack;
EW=1.100; % Nafion equivalent weight [kg/mol]
w=a.lambdam*a.MmH2O*10^(-3)/EW; % Normalized water uptake
SH2=1./(w*1.09*10^5.*exp(77./Tk))*10^5; % Hydrogen solubility in water [mol/m^3/bar]
DH2=1.23*10^(-6)*exp(-(-2602)./Tk); % Hydrogen diffusivity in water [m^2/s]
ppH2=pres-PsatH2O(Tk); % Hydrogen partial pressure [bar]
iH2=SH2.*DH2.*ppH2./lm*2*a.F; % gas crossover current [A/cm^2]
i0_an=a.roughness_an*a.i0ref_an*exp(-(a.Ea_an/a.R).*(1./Tk-1/353));
i0_cat=a.roughness_cat*a.i0ref_cat*exp(-(a.Ea_cat/a.R).*(1./Tk-1/353));
c =a.R.*Tk./(2*a.Alpha.*a.F);
nx=a.R.*Tk.*log(ih2/i0_cat)./a.F; %gas crossover overvoltage [V]
b1=asinh((I./a.A)./(2.*i0_an));
b2=asinh((I./a.A)./(2.*i0_cat));
Vact_deg=c.*(b1+b2)+nx; % [V]
end
```

Ohmic Overvoltage with the Variable Membrane Thickness

```
function VOhm_deg=VOhm_deg(Tk,I,pres,lm)
a=ELCellStack;
```

```matlab
%Area Specific ohmic Resistance
r=lm* 1 ./ (( 0.005139 *a.lambdam + 0.00326 )* exp(1268*(1/303-1./Tk))); % [Ohm*cm^2]
vOhm = ((I/a.A).*r); % [V]
end
```